

AD-A043 460

GRUMMAN AEROSPACE CORP BETHPAGE N Y RESEARCH DEPT
AN ANALYSIS OF THE INVISCID TRANSONIC FLOW OVER TWO-ELEMENT AIR--ETC(U)
JUN 77 B GROSSMAN, G VOLPE

F/G 20/4

N00017-75-C-0722

UNCLASSIFIED

RE-543

ONR-CR215-241-1

NL

1 OF 1
AD
A043460



END
DATE
FILMED
9-77
DDC

AD A 043460

REPORT ONR-CR215-241-1

12



AN ANALYSIS OF THE INVISCID TRANSONIC FLOW
OVER TWO-ELEMENT AIRFOIL SYSTEMS

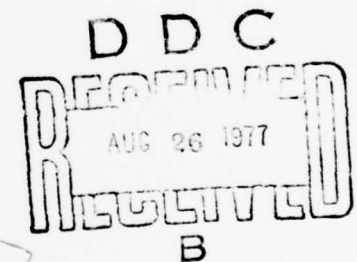
B. GROSSMAN AND G. VOLPE

GRUMMAN AEROSPACE CORPORATION
RESEARCH DEPARTMENT
BETHPAGE, NEW YORK 11714

CONTRACT N00014-75-C-0722

1 JUNE 1977

INTERIM REPORT FOR PERIOD 19 MAY 1975 - 31 DECEMBER 1976



AD No. _____
DDC FILE COPY

Approved for public release; distribution unlimited



PREPARED FOR THE

OFFICE OF NAVAL RESEARCH • 800 N. QUINCY ST. • ARLINGTON • VA • 22217

Change of Address

Organizations receiving reports on the initial distribution list should confirm correct address. This list is located at the end of the report. Any change of address or distribution should be conveyed to the Office of Naval Research, Code 211, Arlington, VA 22217.

Disposition

When this report is no longer needed, it may be transmitted to other organizations. Do not return it to the originator or the monitoring office.

Disclaimer

The findings and conclusions contained in this report are not to be construed as an official Department of Defense or Military Department position unless so designated by other official documents.

Reproduction

Reproduction in whole or in part is permitted for any purpose of the United States Government.

UNCLASSIFIED

SECURITY CLASSIFICATION OF THIS PAGE (When Data Entered)

REPORT DOCUMENTATION PAGE		READ INSTRUCTIONS BEFORE COMPLETING FORM
1. REPORT NUMBER (18) ONR-CR215-241-1 ✓	2. GOVT ACCESSION NO.	3. RECIPIENT'S CATALOG NUMBER (9)
4. TITLE (and Subtitle) An Analysis of the Inviscid Transonic Flow Over Two-Element Airfoil Systems.		5. TYPE OF REPORT & PERIOD COVERED Interim Report. 19 May 1975-31 Dec 1976.
7. AUTHOR(s) (10) B. Grossman G. Volpe		6. PERFORMING ORG. REPORT NUMBER (14) RE-543
9. PERFORMING ORGANIZATION NAME AND ADDRESS Grumman Aerospace Corporation Bethpage, New York 11714		8. CONTRACT OR GRANT NUMBER(s) (15) N00017-75-C-0722
11. CONTROLLING OFFICE NAME AND ADDRESS Office of Naval Research 800 N. Quincy Street Arlington, Virginia 22217		10. PROGRAM ELEMENT, PROJECT, TASK AREA & WORK UNIT NUMBERS
14. MONITORING AGENCY NAME & ADDRESS (if different from Controlling Office) (12) 54p.		12. REPORT DATE (11) 1 June 1977 ✓
		13. NUMBER OF PAGES 51
		15. SECURITY CLASS. (of this report) UNC
		15a. DECLASSIFICATION/DOWNGRADING SCHEDULE
16. DISTRIBUTION STATEMENT (of this Report) Approved for public release; distribution unlimited.		
17. DISTRIBUTION STATEMENT (of the abstract entered in Block 20, if different from Report)		
18. SUPPLEMENTARY NOTES		
19. KEY WORDS (Continue on reverse side if necessary and identify by block number) Transonic Flow, Two-Element Airfoil Systems, Slats, Flaps, Conformal Mapping, Inviscid Irrotational Flow.		
20. ABSTRACT (Continue on reverse side if necessary and identify by block number) This report describes the development of a method for numerically computing the inviscid transonic flow field over an airfoil with a leading-edge slat or a trailing-edge flap. The approach is to solve the full inviscid irrotational flow equations about two-element airfoil systems. The methodology consists of the development of a suitable computational plane and grid system through the application of a series of conformal mappings. The		

DD FORM 1 JAN 73 1473

EDITION OF 1 NOV 65 IS OBSOLETE
S/N 0102-014-6601

UNCLASSIFIED 406 165

SECURITY CLASSIFICATION OF THIS PAGE (When Data Entered)

LB

UNCLASSIFIED

SECURITY CLASSIFICATION OF THIS PAGE (When Data Entered)

20 continued.

appropriate set of equations and boundary conditions are derived in terms of a smoothly varying, single-valued reduced potential function through analytic removal of all singularities in the computational domain. A stable and accurate relaxation procedure is established for the numerical solution of the governing equations. The method is applied to a variety of transonic supercritical two-element airfoil configurations. Results are presented depicting the surface pressure distribution, streamline patterns in the physical and computational domain, and Mach number contours.

ACCESSION for	
NTIS	White Section <input checked="" type="checkbox"/>
DDC	Buff Section <input type="checkbox"/>
UNANNOUNCED	<input type="checkbox"/>
JUS T I C A T I O N	
FY	
D I S T R I B U T I O N / A V A I L A B I L I T Y C O D E S	
01	and/or SPECIAL
A	

UNCLASSIFIED

SECURITY CLASSIFICATION OF THIS PAGE (When Data Entered)

Report ONR-CR215-241-1
RE-543

AN ANALYSIS OF THE INVISCID TRANSONIC FLOW OVER
TWO-ELEMENT AIRFOIL SYSTEMS

Interim Report for Period 19 May 1975-31 December 1976

by

B. Grossman and G. Volpe

Prepared Under Contract N00014-75-C-0722

for


Office of Naval Research
800 N. Quincy St.
Arlington, VA 22217

by

Research Department
Grumman Aerospace Corporation
Bethpage, New York 11714

June 1977

Approved by


Richard A. Schelling
Director of Research

PREFACE

The authors gratefully express their appreciation to Dr. R. E. Melnik of the Grumman Research Department and Professor A. Jameson of NYU for their very helpful discussions on various aspects of this problem. We also acknowledge the assistance of Mr. Frank Koch II of the Grumman Research Department for his help with some of the computational difficulties occurring in the course of this work.

ABSTRACT

This report describes the development of a method for numerically computing the inviscid transonic flow field over an airfoil with a leading-edge slat or a trailing-edge flap. The approach is to solve the full inviscid irrotational flow equations about two-element airfoil systems. The methodology consists of the development of a suitable computational plane and grid system through the application of a series of conformal mappings. The appropriate set of equations and boundary conditions are derived in terms of a smoothly varying, single-valued reduced potential function through analytic removal of all singularities in the computational domain. A stable and accurate relaxation procedure is established for the numerical solution of the governing equations. The method is applied to a variety of transonic supercritical two-element airfoil configurations. Results are presented depicting the surface pressure distribution, streamline patterns in the physical and computational domains, and Mach number contours.

TABLE OF CONTENTS

<u>Section</u>	<u>Page</u>
1 Introduction	1
2 Mappings	3
3 Mathematical Formulation.	13
4 Numerical Formulation	17
5 Results	22
6 Conclusions	36
7 References	37
Appendix - Determination of the Z_3 - Z_4 Mapping Coefficients	38

LIST OF ILLUSTRATIONS

<u>Figure</u>	<u>Page</u>
1 Sequence of Conformal Mappings	4
2 Computational Domain.	9
3 Annular Domain	10
4 Coordinate Grid-Physical Plane NACA 23012 Airfoil/2H flap	11
5 Coordinate Grid-Physical Plane Clark Y Airfoil/30% Maxwell Slat	12
6 Computed Surface Pressure Distribution-NACA 23012 Airfoil/2H Flap, $M_\infty = 0.5$, $\alpha = 4^\circ$	23
7 Computed Streamlines-Annular Domain NACA 23012 Airfoil/2H Flap, $M_\infty = 0.5$, $\alpha = 4^\circ$	24
8 Computed Streamlines-Physical Plane NACA 23012 Airfoil/2H Flap, $M_\infty = 0.5$, $\alpha = 4^\circ$	25
9 Computed Surface Pressure Distribution-Clark Y Airfoil/30% Maxwell Slat, $M_\infty = 0.6$, $\alpha = 6^\circ$	26
10 Computed Streamlines-Annular Domain Clark Y Airfoil/30% Maxwell Slat, $M_\infty = 0.6$, $\alpha = 6^\circ$	27
11 Computed Streamlines-Physical Plane Clark Y Airfoil/30% Maxwell Slat, $M_\infty = 0.6$, $\alpha = 6^\circ$	27
12 Computed Surface Pressure Distribution-Modified NACA 64A008 Airfoil/ Slat, $M_\infty = 0.7$, $\alpha = 6^\circ$	28
13 Computed Streamlines-Physical Domain Modified NACA 64A008 Airfoil/ Slat, $M_\infty = 0.7$, $\alpha = 6^\circ$	29
14 Computed Surface Pressure Distribution-Modified NACA 64A009 Airfoil/ Slat, $M_\infty = 0.8$, $\alpha = 4^\circ$	30
15 Mach Number Contours-Modified NACA 64A009 Airfoil/Slat, $M_\infty = 0.8$, $\alpha = 4^\circ$	31
16 Mach Number Contours-NACA 0012 Airfoil and Slat, $M_\infty = 0.6$, $\alpha = 4^\circ$	32
17 Computed Surface Pressure Distribution-NACA 0012 Airfoil and Slat, $M_\infty = 0.6$, $\alpha = 4^\circ$	33
18 Computed Surface Pressure Distribution-NACA 64A406 Airfoil/7.8A Slat, $M_\infty = 0.649$, $\alpha = 4^\circ$	34
19 Mach Number Contours-NACA 64A406 Airfoil/7.8A Slat, $M_\infty = 0.649$, $\alpha = 4^\circ$	35

LIST OF SYMBOLS

a	local speed of sound
E_1	defined by Eq. (23)
E_2	defined by Eq. (24)
f	defined by Eq. (15)
G	reduced potential
H	metric of conformal mappings
\tilde{H}	reduced metric
i	index for difference expressions, X direction
j	index for difference expressions, Y direction
k, k_1, k_2	mapping constants, Eq. (13)
L	defined by Eq. (22)
M	Mach number
N	local coordinate normal to Streamlines computational domain
q	magnitude of velocity
r	radial direction in annular domain
r_s	radius of inner ring corresponding to secondary airfoil in annular domain
r_∞	radius of point of infinity in annular domain
S	local streamwise coordinate, computational domain velocity component in r direction
u	velocity component in r direction
u_1	defined by Eq. (27)
v	velocity component in θ direction
v_1	defined by Eq. (28)
X	stretched θ coordinate-computational domain
Y	stretched r coordinate-computational domain
Z_1	complex physical domain
Z_2-Z_5	intermediate mapped domains
Z_6	complex annular domain, $= re^{i\theta}$

α	angle of attack
β	defined by Eq. (18)
γ	ratio of specific heats
Γ_1, Γ_2	circulation constants for main and secondary airfoils
δG_j	$= G_j - G_j^o$
ΔX	mesh spacing, X direction
ΔY	mesh spacing, Y direction
θ	azimuthal direction in annular domain
Φ	complete potential function
Φ_1	free-stream contribution to potential
Φ_2	circulatory flow contribution to potential
Φ_3	additional circulatory flow contribution to potential
Superscripts	
o	old value in iterative relaxation process
$'$	derivative of stretching functions with respect to their arguments
Subscripts	
i	index for difference expression in X direction
j	index for difference expression in Y direction
∞	free stream quantity

1. INTRODUCTION

In order for an aircraft to maneuver effectively in the transonic speed range, its wing must generate high lift coefficients without incurring excessive drag or buffeting. The recent development of supercritical wings can enable a designer to meet this specification. However, this requirement will often degrade the aircraft's performance at cruising speeds with larger than optimal drag coefficients. The implementation of high lift devices at transonic speeds offers the possibility of greatly enhancing the maneuvering capabilities of modern aircraft without compromising their cruising efficiency. This possibility has been proven in the last few years by the installation of slats on the F-4 and the positive test of a slatted wing on the F-14 aircraft. The performance of these aircraft in managing climbs and turns at transonic speeds was remarkably improved by the presence of the slats, even though these configurations have not been shown to be optimal by any means.

The aerodynamic designer currently lacks an analytical tool to design, or even analyze, transonic airfoils with high lift devices. Furthermore, the paucity of experimental data currently makes it difficult to determine what can be achieved with these maneuvering devices. Also, the experimental gathering of data on such configurations would be tremendously expensive in light of the number of configurations that would need to be tested and the high speeds and Reynolds numbers required in a wind tunnel test. A theoretical tool for the analysis of the transonic flow over a two-element airfoil system would be a first valuable step in aiding the designer in his task by cutting down on the number of configurations to be tested and providing insight into the flow phenomena that are present at high speeds.

This report describes the development of a method for numerically computing the inviscid transonic flow over an airfoil with a leading-edge slat or a trailing-edge flap. In general, these flow fields are difficult to obtain analytically because of the complicated geometry of the multiply connected domain. Small disturbance approximations (such as those used for this problem in Ref. 1) do not appear to be adequate since the interaction of the flow between the airfoils will provide large perturbations to the flow field.

In recent years the application of mixed-flow relaxation techniques, introduced by Murman and Cole (Ref. 2), has made possible the numerical computation of inviscid transonic

flows over a variety of geometrical shapes in both two and three dimensions. These methods are generally based on the assumption of irrotational flow and solve either the full potential equation or an appropriate form of the small disturbance equation. For two-dimensional flows in particular, accurate and efficient solutions to the full potential equation have been obtained for transonic flows over airfoil sections (Refs. 3, 4), over axisymmetric bodies (Refs. 5, 6), and over nacelles (Refs. 7, 8).

In this report these relaxation techniques are applied to determine the flow about an airfoil with a slat or a flap at transonic speeds. The approach is to solve the full inviscid, irrotational flow equations about two-element airfoil systems. The methodology consists of the 1) development of a suitable computational plane and grid system, 2) evaluation of an appropriate set of governing inviscid equations and boundary conditions in terms of smoothly varying, single-valued functions in the computational domain, and 3) establishment of a stable and accurate numerical procedure for the solution of the governing equations.

An abbreviated version of this analysis was presented at an International Symposium (Ref. 9) and this report is designed to provide the details of the method. Arlinger (Ref. 10) has recently developed independently a similar inviscid analysis of this problem.

The method will provide solid groundwork for the development of a computational tool that includes viscous corrections, and one that actually designs two-element airfoil systems: a numerical computation that generates airfoil ordinates when a desired pressure distribution is specified over part or the whole of the configuration.

2. MAPPINGS

A crucial step in the development of a finite difference method to compute flows over complicated geometries is to develop a suitable grid system. It is highly desirable to have the geometric contours aligned with a coordinate line in order to avoid interpolations and extrapolations in applying the surface boundary conditions. It is also convenient for external flow problems to map the infinite physical domain to a finite computational space in order to apply accurately the far-field boundary conditions. Furthermore, the mappings should concentrate grid lines in regions of steep flow gradients such as airfoil leading and trailing edges and in the slot formed between the main airfoil and the slat or flap.

In our approach, we use analytic and numerical conformal mapping methods to transform the infinite domain external to the two-element airfoil system to the annular region between two concentric circular rings. The outer ring corresponds to the main airfoil surface and the inner ring to the secondary airfoil surface (flap or slat). Infinity in the physical plane is mapped to a single point with the circular annulus in the computational domain. The mapping method follows from the work of Ives (Ref. 11) and utilizes a sequence of five conformal transformations, three analytic and two numerical. We briefly summarize below the details of the mapping as they have been used in our approach.

The first step consists of mapping the main airfoil to a near circle using a von Karman-Trefftz transformation, as illustrated in Figs. 1a and 1b. Denoting the physical plane as $Z_1 = x_1 + iy_1$, the first mapped plane Z_2 becomes

$$\frac{Z_2 - S}{Z_2 + S} = \left(\frac{Z_1 - Z_{1T}}{Z_1 - Z_{1N}} \right)^{1/\kappa_1} \quad (1)$$

where Z_{1T} is the location of the trailing edge, Z_{1N} is located inside the airfoil at a point midway between the nose and its center of curvature, $\kappa_1 = 2 - \tau_1/\pi$ with τ_1 being the included trailing edge angle of the main airfoil and $S = (Z_{1T} - Z_{1N})/2\kappa_1$.

The second step is a Theodorsen-Garrick transformation utilizing fast Fourier transforms to map the main airfoil near circle to an exact circle. The next mapped plane, Z_3 , illustrated in Fig. 1c is

$$Z_2 - Z_{2c} = Z_3 \exp \left\{ \sum_{j=0}^N (A_j + iB_j) Z_3^{-j} \right\} \quad (2)$$

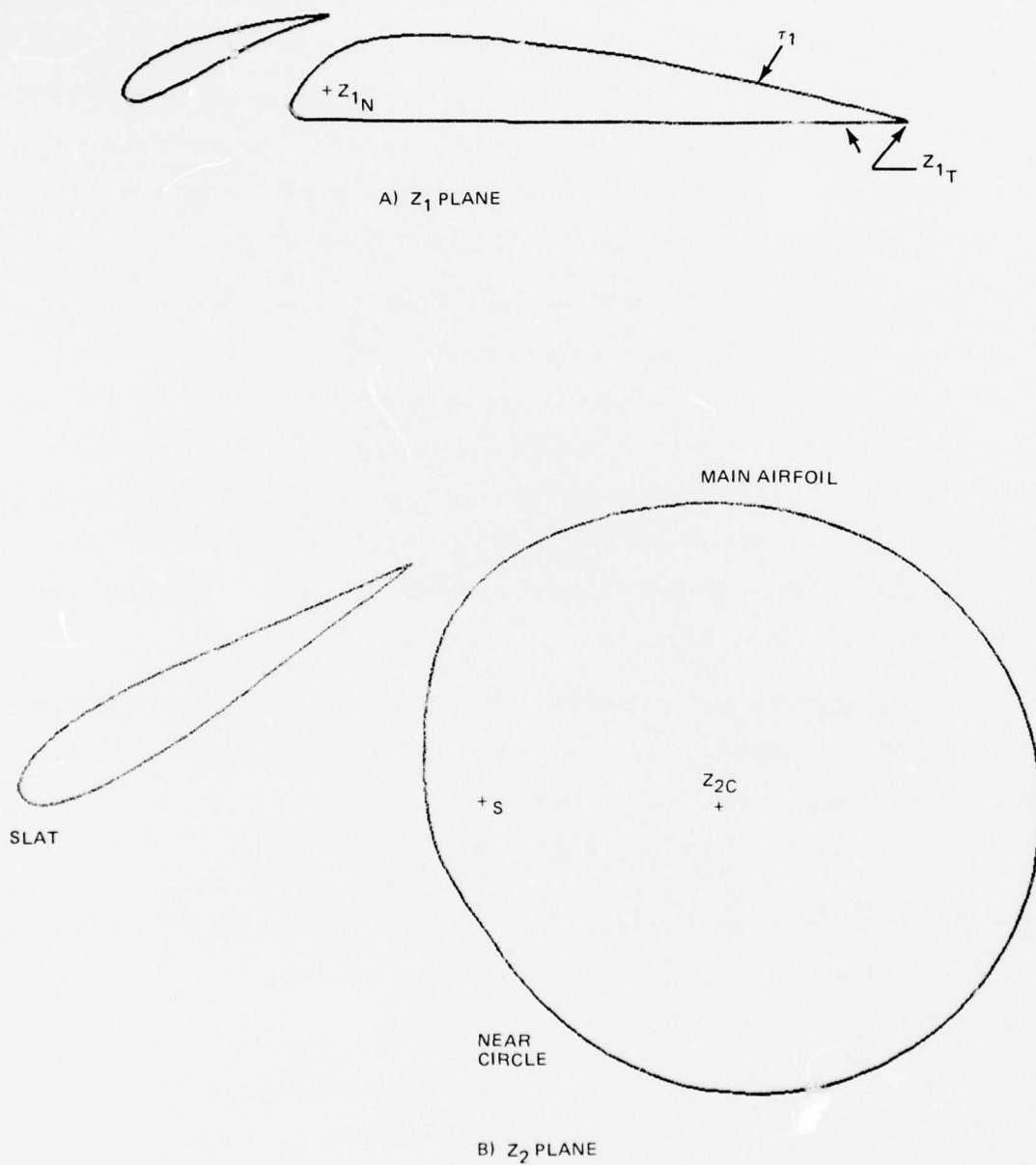


Fig. 1 Sequence of Conformal Mappings

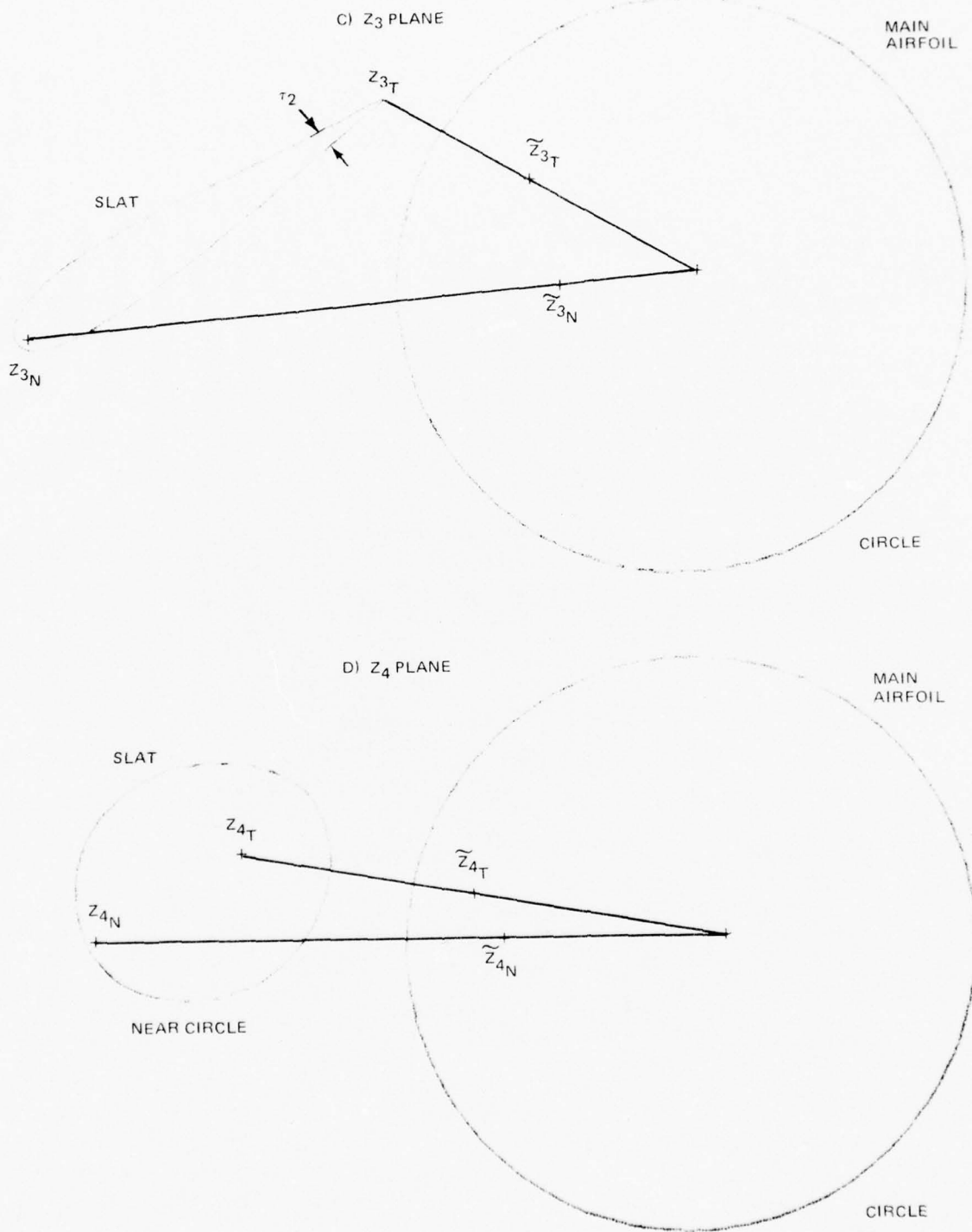


Fig. 1 Sequence of Conformal Mappings (continued)

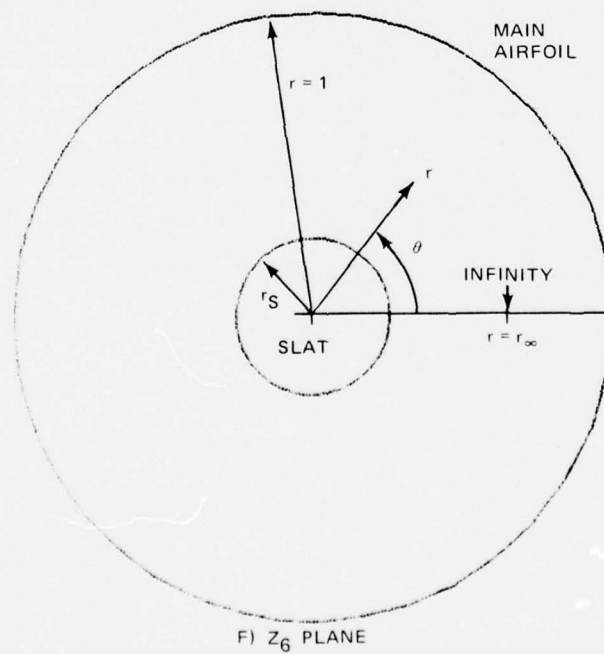
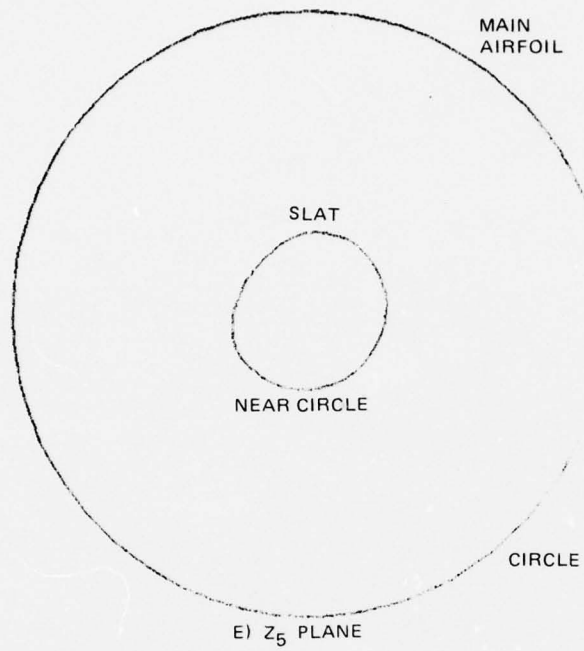


Fig. 1 Sequence of Conformal Mappings (continued)

where Z_{2c} is the location of the centroid of the near circular image of the main airfoil in the Z_2 plane and A_i and B_i are constants which are determined iteratively as discussed in Ref. 11.

The third step of the mapping is an analytic transformation of the secondary airfoil to a near circle, which keeps the image of the main airfoil a circle (but of different radius). The transformation to the Z_4 plane is written as

$$\frac{(Z_4 - Z_{4T})(Z_4 - \bar{Z}_{4T})}{(Z_4 - Z_{4N})(Z_4 - \bar{Z}_{4N})} = \left[\frac{(Z_3 - Z_{3T})(Z_3 - \bar{Z}_{3T})}{(Z_3 - Z_{3N})(Z_3 - \bar{Z}_{3N})} \right]^{1/\kappa_2} \quad (3)$$

where

$$\begin{aligned} \bar{Z}_{3T} &= 1/\bar{Z}_{3T} \\ \bar{Z}_{3N} &= 1/\bar{Z}_{3N} \\ \bar{Z}_{4T} &= r_s^2/\bar{Z}_{4T} \\ \bar{Z}_{4N} &= r_s^2/\bar{Z}_{4N} \\ \kappa_2 &= 2 - \tau_2/\pi \end{aligned}$$

and r_s is the radius of the circle corresponding to the main airfoil in the Z_4 plane and τ_2 is the included trailing edge angle of the secondary airfoil. In a manner similar to the $Z_1 - Z_2$ mapping, the singular points Z_{3T} and Z_{3N} are placed at the trailing edge and midway between the nose and its center of curvature as illustrated in Fig. 1d. The unknown constants in Eq. (3) are Z_{4T} , Z_{4N} and r_s . Our procedure for the evaluation of these constants differs from Ives (Ref. 11) and is detailed in the appendix.

The fourth step of the mapping consists of using a bilinear transformation to place the new circular image of the secondary airfoil at the center of main airfoil circle as illustrated in Fig. 1e. The mapping takes the form

$$Z_5 = A \frac{Z_4 + B}{Z_4 + C} \quad (4)$$

where the procedure for computing the constants A, B, and C is found in Ref. 11.

The fifth transformation of the two concentric shapes to two circular rings is performed through a second application of a Theodorsen-Garrick mapping of the form

$$Z_5 = Z_6 \exp \left\{ iD_0 + \sum_{j=0}^N \left[(-C_j + iD_j)(r_s Z_6)^j + (C_j + iD_j)(r_s/Z_6)^j \right] \right\}. \quad (5)$$

As shown in Fig. 1f, taking $Z_6 = re^{i\theta}$, the main airfoil lies exterior to the circle $r = 1$, the secondary airfoil lies interior to $r = r_s$ and the point of infinity is at $r = r_\infty$, $\theta = 0$.

A further set of transformations $X = X(\theta)$ and $Y = Y(r)$ is used to obtain the final computational domain. It is convenient to have the point of infinity $r = r_\infty$ located at a fixed grid point in the computational domain, since boundary values must be applied there. Hence, we take $Y(r_\infty) = 1/2$ and define a parabolic transformation by

$$r - r_s = (A_1 Y + A_2) Y \quad (6)$$

where

$$A_1 = 2(1 - 2r_\infty + r_s)$$

$$A_2 = 4r_\infty - 3r_s - 1$$

The main airfoil is located at $Y = 1$, the secondary airfoil at $Y = 0$, and the point at infinity is at $Y = 1/2$.

In the azimuthal direction we introduce a mapping $X = X(\theta)$ in order to give some control on the concentration of grid lines and to locate the trailing edges at grid points in the computational space. This latter requirement will allow an accurate imposition of the Kutta condition at the trailing edges. The mapping consists of two steps; first to produce desired mesh spacings

$$\theta = E \sin \phi + F \sin 2\phi + G \quad (7)$$

where the constants E, F, G are arbitrary, subjected to the constraints

$$E < 4/3 \quad F < 1/6$$

The final step of locating each trailing edge and the point of infinity at grid lines is obtained through

$$2\pi [\phi(\theta) - \phi_0] = X + B_1 \sin 2\pi X + B_2 (\cos 2\pi X - 1) \quad (8)$$

where

$$B_1 = -\frac{1}{2} \left[\frac{(\bar{\phi}_1 - X_1) \sin \pi X_2}{\sin \pi X_1 \sin \pi(X_1 - X_2)} + \frac{(\bar{\phi}_2 - X_2) \sin \pi X_1}{\sin \pi X_2 \sin \pi(X_2 - X_1)} \right]$$

$$B_2 = -\frac{1}{2} \left[\frac{(\bar{\phi}_1 - X_1) \cos \pi X_2}{\sin \pi X_1 \sin \pi(X_1 - X_2)} + \frac{(\bar{\phi}_2 - X_2) \cos \pi X_2}{\sin \pi X_2 \sin \pi(X_2 - X_1)} \right]$$

and $\bar{\phi}_1 = 2\pi [\phi(\theta_{T1}) - \phi_0]$, $\bar{\phi}_2 = 2\pi [\phi(\theta_{T2}) - \phi_0]$, $\phi_0 = \phi(0)$ and θ_{T1} and θ_{T2} are the trailing edge locations of the main and secondary airfoils, respectively. The values X_1 and X_2 correspond to fixed mesh points for the trailing edges and $X = 0$ corresponds to the location in the θ plane ($\theta = 0$) of the point of infinity.

The final computational domain is sketched in Fig. 2. In this plane a uniform grid produces the mesh distribution in the annular domain shown in Fig. 3 and in the physical domain shown in Figs. 4 and 5 for typical flap and slat configurations. The mapping produces a grid where each airfoil surface is a coordinate line, the trailing edges occur on mesh points and with a high density of grid lines in the slot region and near all stagnation points. Although the mapping procedure is quite complicated, our computer program to calculate the coefficients of all the terms generally requires less than 10 seconds on an IBM 370/168.

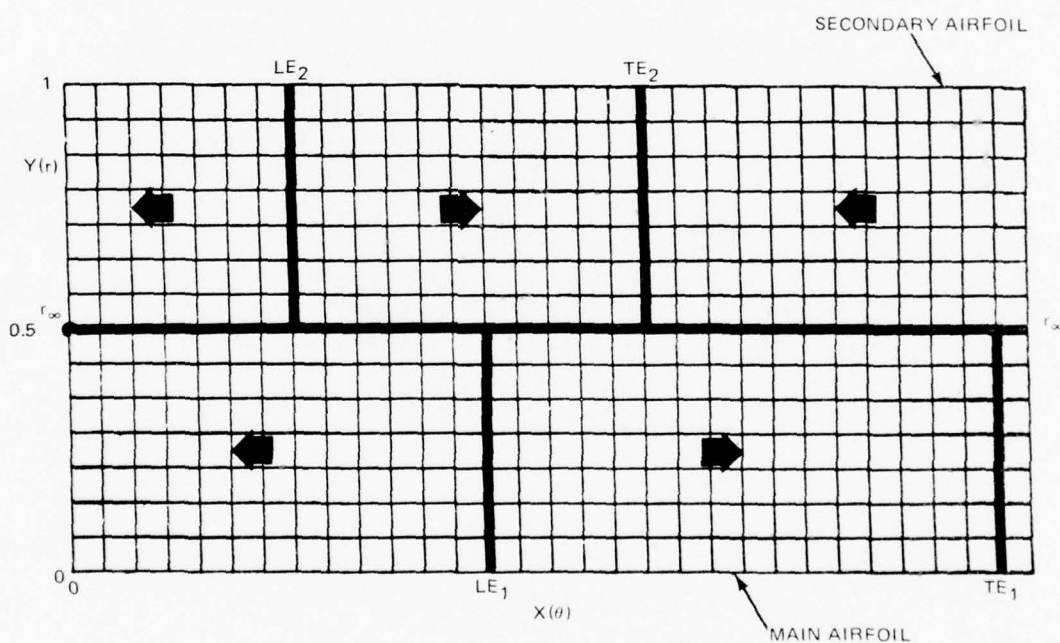


Fig. 2 Computational Domain

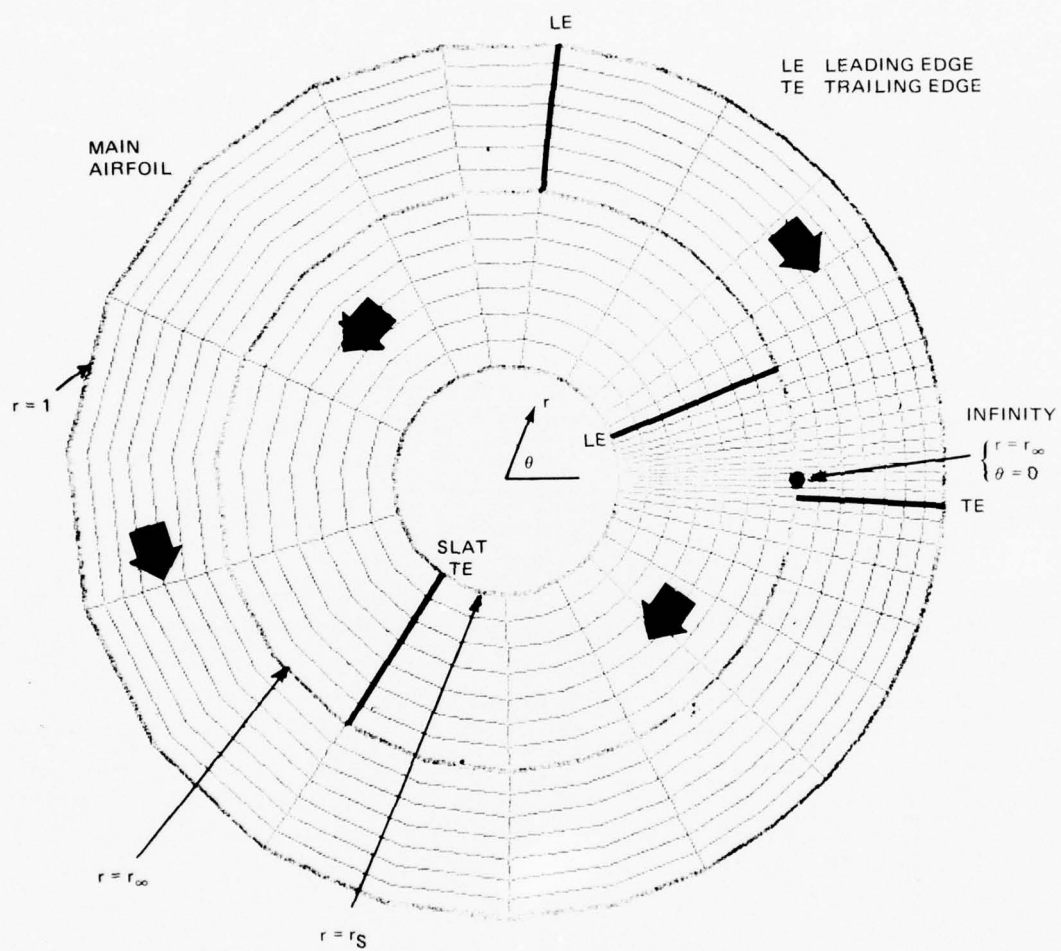


Fig. 3 Annular Domain

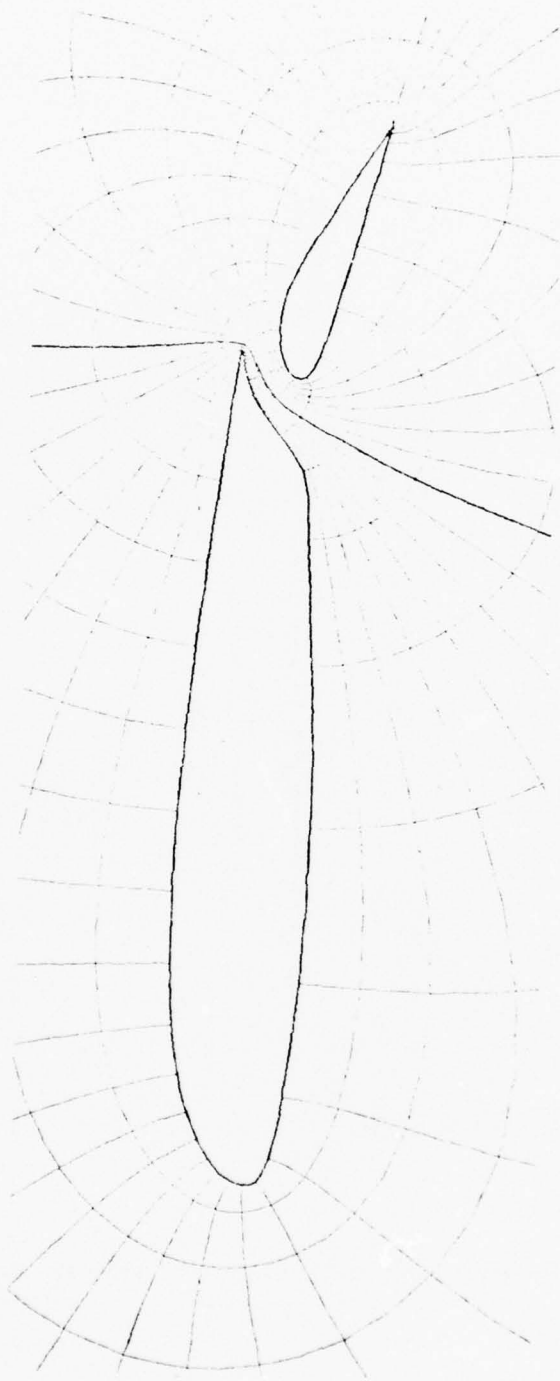


Fig. 4 Coordinate Grid — Physical Plane NACA 23012 Airfoil/2H Flap

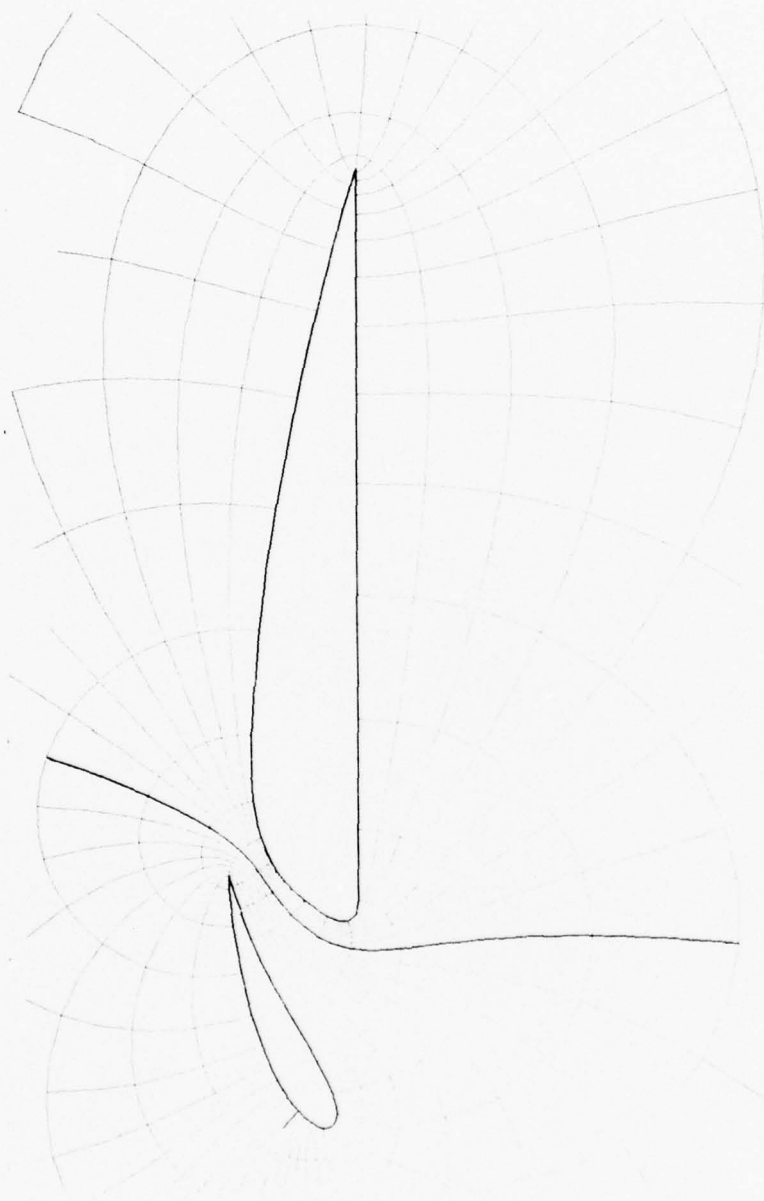


Fig. 5 Coordinate Grid – Physical Plane Clark Y Airfoil/30% Maxwell Slat

3. MATHEMATICAL FORMULATION

The governing equations for the inviscid, irrotational, compressible flow about a two-element airfoil system are written in the annular domain $Z_6 = re^{i\theta}$ using the metric H of the conformal mappings, Eqs. (1)–(5), in terms of a potential function Φ , as

$$(a^2 - v^2)\Phi_{rr} - \frac{2uv}{r}\Phi_{r\theta} + (a^2 - u^2)\frac{1}{r^2}\Phi_{\theta\theta} + (a^2 + u^2)\frac{1}{r}\Phi_r + (v^2 + u^2)\left(vH_r + \frac{u}{r}H_\theta\right) = 0 \quad (9)$$

and

$$a^2 = \frac{1}{M_\infty^2} + \frac{(\gamma - 1)}{2} (1 - u^2 - v^2) \quad (10)$$

where

$$v = \frac{1}{H}\Phi_r$$

$$u = \frac{1}{rH}\Phi_\theta$$

$$H = \left| \frac{dZ_1}{dZ_6} \right|$$

and M_∞ is the free stream Mach number and γ the ratio of specific heats. The boundary condition on the surface of the airfoils is

$$\Phi_r = 0 \quad \text{on } r = r_s \text{ and } r = 1 \quad (11)$$

At the airfoil trailing edges, since the metric H goes to zero, the Kutta condition that requires there be no flow around the trailing edges, may be expressed as

$$\Phi_\theta = 0 \quad \text{at both trailing edges.} \quad (12)$$

Singularities in the above formulation are seen to arise for several reasons. First, the metric of the mapping becomes unbounded at infinity ($r = r_\infty$, $\theta = 0$). It can be shown that near infinity

$$\frac{dZ_1}{dZ_6} \rightarrow \frac{K}{(Z_6 - r_\infty)^2} \quad \text{as } Z_6 \rightarrow r_\infty \quad (13)$$

and K is a known complex constant which can be taken to be $K = k_1 e^{ik_2}$. The metric may then be regularized by

$$H = \frac{k_1}{f} \tilde{H} \quad (14)$$

where

$$f \equiv |Z_6 - r_\infty|^2 = r^2 - 2r_\infty r \cos \theta + r_\infty^2 \cos^2 \theta \quad (15)$$

and \tilde{H} is a smooth bounded function which goes to unity at $Z_6 = r_\infty$.

Next, the potential function itself becomes unbounded and multivalued near the point of infinity in the computational domain. One contribution to the singular potential comes from the behavior of the uniform flow near infinity, which can be shown to be of the form, for $Z_6 \rightarrow r_\infty$

$$\Phi_1(r, \theta) = \text{Real} \left\{ \frac{-k e^{i\alpha}}{Z_6 - r_\infty} \right\} = -\frac{k_1}{f} [r \cos(\theta + \alpha - k_2) - r_\infty \cos(\alpha - k_2)] \quad (16)$$

where α is the angle of attack of the free stream velocity vector.

A second contribution to the singular potential comes from the multivalued nature of the circulatory flow near infinity in the annular domain. In taking a closed circuit about $Z_6 = r_\infty$, the potential must jump by 2π times the circulation about each airfoil. The solution for the circulatory flow potential valid near infinity is found as a solution to the Prandtl-Glauert equations (see Ref. 12) and is transformed to the computation domain as

$$\Phi_2(r, \theta) = -(\Gamma_1 + \Gamma_2) \tan^{-1} [\sqrt{1 - M_\infty^2} \tan \beta] \quad (17)$$

where

$$\beta = k_2 - \alpha + \pi - \tan^{-1} \left(\frac{r \sin \theta}{r \cos \theta - r_\infty} \right) \quad (18)$$

and Γ_1 and Γ_2 are equal to 2π times the circulation constants about the main and secondary airfoils, respectively.

To obtain a single-valued reduced potential, another term Φ_3 must be added to Φ_2 so that any closed contours about individual airfoils will produce the required circulation jump. This is obtained through a term

$$\Phi_3 = -\Gamma_2 \theta \quad (19)$$

A reduced potential function $G(r, \theta)$ may now be defined which remains bounded and single-valued throughout the entire annular domain as

$$G(r, \theta) = \Phi - \Phi_1 - \Phi_2 - \Phi_3 \quad (20)$$

The governing equation for the reduced potential is then obtained by introducing Eqs. (14)–(20) into Eq. (9), whereby

$$(a^2 - v^2)fG_{rr} - \frac{2uv}{r}f\left[G_{r\theta} - \frac{1}{r}(G_\theta - \Gamma_2)\right] + (a^2 - u^2)\frac{f}{r}\left(\frac{1}{r}G_{\theta\theta} + G_r\right) + (u^2 + v^2)k_1\left(v\tilde{H}_r + \frac{u}{r}\tilde{H}_\theta\right) + L = 0 \quad (21)$$

and

$$\begin{aligned} L \equiv & -\frac{4uv}{r}\left[(r - r_\infty \cos \theta)(G_\theta - \Gamma_2) + r r_\infty \sin \theta G_r\right] \\ & + 2(u^2 - v^2)\left[(r - r_\infty \cos \theta)G_r - \frac{r_\infty}{r} \sin \theta (G_\theta - \Gamma_2)\right] \\ & - (\Gamma_1 + \Gamma_2)\frac{E_1}{f}\left\{2(u^2 - v^2)(r - r_\infty \cos \theta)r_\infty \sin \theta + 2uv(f - 2r_\infty^2 \sin^2 \theta)\right. \\ & \left. - E_2[a^2 f - (r_\infty v \sin \theta + r_\infty u \cos \theta - ur)^2]\right\} \end{aligned} \quad (22)$$

where

$$E_1 \equiv \frac{\sqrt{1 - M_\infty^2}}{1 - M_\infty^2 \sin^2 \beta} \quad (23)$$

$$E_2 \equiv \frac{-M_\infty^2 \sin 2\beta}{1 - M_\infty^2 \sin^2 \beta} \quad (24)$$

and f and β are defined in Eqs. (15) and (18), respectively. The radial and circumferential velocity components, v and u become

$$v = \frac{1}{\tilde{H}k_1}\left\{fG_r - (\Gamma_1 + \Gamma_2)E_1 r_\infty \sin \theta + v_1\right\} \quad (25)$$

$$u = \frac{1}{\tilde{H}k_1}\left\{\frac{f}{r}(G_\theta - \Gamma_2) - (\Gamma_1 + \Gamma_2)E_1(r_\infty \cos \theta - r) + u_1\right\} \quad (26)$$

where

$$v_1 \equiv \frac{k_1}{f}\left[r^2 \cos(\theta + \alpha - k_2) - 2r r_\infty \cos(\alpha - k_2) + r_\infty^2 \cos(\theta - \alpha + k_2)\right] \quad (27)$$

$$u_1 \equiv \frac{k_1}{f}\left[r^2 \sin(\theta + \alpha - k_2) - 2r r_\infty \sin(\alpha - k_2) - r_\infty^2 \sin(\theta - \alpha + k_2)\right] \quad (28)$$

The boundary condition of the vanishing of normal velocity on the surface of the airfoils, Eq. (11) becomes

$$G_r = \frac{1}{f}\left[(\Gamma_1 + \Gamma_2)E_1 r_\infty \sin \theta - v_1\right] \quad \text{at } r = r_s \text{ and } r = 1 \quad (29)$$

The Kutta condition, Eq. (12) becomes

$$\Gamma_1 E_1(r_\infty \cos \theta - r) + \Gamma_2 \left[\frac{f}{r} + E_1(r_\infty \cos \theta - r) \right] = \frac{f}{r} G_\theta + u_1 \quad (30)$$

at each trailing edge. This gives to two linear expressions for Γ_1 and Γ_2 which can be solved at each step in the iterative numerical solution.

An additional boundary condition must be enforced at the point representing infinity. The entire solution there is given by the sum of the free stream and circulatory flows. No additional velocities must be generated by reduced potential G . So, in effect, G must be a constant at infinity and, therefore, a constant in all directions at $r = r_\infty$, $\theta = 0$. For convenience this constant is chosen as zero.

Solutions to the boundary value problem comprising Eqs. (10), (21)–(30), can be obtained by iteration and the numerical scheme will be described in the following section. A starting point for the iteration process is provided by Legally's solution (Ref. 13) for the incompressible flow over two circular cylinders, which in terms of the reduced potential $G(r, \theta)$ may be written as

$$\begin{aligned} G(r, \theta) = \text{Real} \left\{ -k_1 \left[\frac{e^{-i(k_2 - \alpha)} Z_6}{1 - r_\infty Z_6} + \sum_{j=1} \frac{e^{-i(k_2 - \alpha)}}{r_\infty} \left(\frac{r_\infty Z_6 r_s^{2j}}{1 - r_\infty Z_6 r_s^{2j}} - \frac{\frac{1}{r_\infty Z_6} r_s^{2j}}{1 - \frac{1}{r_\infty Z_6} r_s^{2j}} \right) \right. \right. \\ \left. \left. + \sum_{j=1} \frac{e^{i(k_2 - \alpha)}}{r_\infty} \left(\frac{\frac{r_\infty}{Z_6} r^{2j}}{1 - \frac{r_\infty}{Z_6} r^{2j}} - \frac{\frac{Z_6}{r_\infty} r^{2j}}{1 - \frac{Z_6}{r_\infty} r^{2j}} \right) \right] \right. \\ \left. - i(\Gamma_1 + \Gamma_2) \left[-\log(1 - r_\infty Z_6) + \sum_{j=1} \log \frac{\left(1 - \frac{r_\infty}{Z_6} r^{2j}\right) \left(1 - \frac{Z_6}{r_\infty} r^{2j}\right)}{\left(1 - r_\infty Z_6 r^{2j}\right) \left(1 - \frac{1}{r_\infty Z_6} r^{2j}\right)} \right] \right\} \quad (31) \end{aligned}$$

4. NUMERICAL FORMULATION

The Neumann boundary value problem formulated in the preceding sections is solved numerically using the ideas and techniques developed for mixed subsonic and supersonic flows about a single airfoil. The reduced potential equation, Eq. (21), is solved by a successive column-relaxation algorithm utilizing type-dependent differencing originated by Murman and Cole (Ref. 2). However, the sequences of mappings produces a computational plane in which the coordinate lines are not aligned with the streamwise direction. Jameson's technique (Ref. 14) for developing a coordinate invariant or "rotated" difference scheme proves valuable in the numerical formulation of this problem.

The solution of the flow field is obtained by replacing the potential equation with a finite-difference analog at each point in the grid. The resulting set of difference equations is solved by iteration, a process which can be regarded as a sequence of steps in an artificial time coordinate frame. During each iteration the updating of an initial potential field is accomplished simultaneously at a number of points on the same column ($X = \text{constant}$) and sweeping, column by column, through the computational grid. It is imperative that the flow field be swept in a direction which is no more than 90° from the streamwise direction in order to retain the proper domain of dependence everywhere. A scheme which has proved suitable in this problem has been to divide the flow field in two by the coordinate ring passing through the infinity point ($r = r_\infty$ or $Y \approx \frac{1}{2}$). Each half of the total field can then be considered to surround a single element and is swept from the leading edge to the trailing edge of the airfoil along one surface, and then along the other as illustrated in Figs. 2 and 3. A column of points extending from the surface to the middle coordinate ring is thus updated at each pass. At the end of each sweep the Kutta condition at each airfoil trailing edge is enforced by solving for the circulation values, Γ_1 and Γ_2 , which satisfy the difference equations corresponding to Eq. (30).

Before Eq. (21) can be used for numerical simulation it should be re-written in terms of the working coordinates X and Y . Since $\theta = \theta(X)$ and $r = r(Y)$ defined in Eqs. (6)–(8),

$$G_\theta = \frac{dX}{d\theta} G_X = X' G_X$$

$$G_{\theta\theta} = X'^2 G_{XX} + X'' G_X$$

$$G_r = \frac{dY}{dr} G_Y = Y' G_Y$$

$$G_{rr} = Y'^2 G_{YY} + Y'' G_Y$$

$$G_{r\theta} = X' Y' G_{XY}$$

Similar expressions can be written for \tilde{H}_r and \tilde{H}_θ ; Eq. (20) then can be put in the form

$$A_1 G_{XX} + A_2 G_{XY} + A_3 G_{YY} + A_4 G_X + A_5 G_Y + A_6 = 0 \quad (31)$$

where

$$A_1 = (a^2 - u^2) \frac{fX'^2}{r^2}$$

$$A_2 = -2uv \frac{fX'Y'}{r}$$

$$A_3 = (a^2 - v^2) fY'^2$$

$$A_4 = 2uv \left[\frac{fX'}{r^2} - 2(r - r_\infty \cos \theta) \frac{X'}{r} \right] + (a^2 - u^2) \frac{fX''}{r^2} - 2(u^2 - v^2) r_\infty \sin \theta \frac{X'}{r}$$

$$A_5 = -4uv r_\infty \sin \theta Y' + (a^2 - v^2) fY'' + (a^2 - u^2) \frac{fY'}{r} + 2(u^2 - v^2)(r - r_\infty \cos \theta) Y'$$

$$A_6 = (u^2 + v^2) k_1 \left(u \tilde{H}_X \frac{X'}{r} + v Y' \tilde{H}_Y \right) + \Gamma_2 \left[\frac{2r_\infty \sin \theta}{r} (u^2 - v^2) - 2uv \left(\frac{r_\infty^2}{r^2} - 1 \right) \right] \\ + 2E_1 [r_\infty \sin \theta (r - r_\infty \cos \theta) (u^2 - v^2) + uv(f - 2r_\infty^2 \sin^2 \theta)] \\ + E_1 E_2 \{ [u(r_\infty \cos \theta - r) + v r_\infty \sin \theta]^2 - a^2 f \}$$

Finite-difference analogs of the potential equation are constructed following the rules developed for the single airfoil problem. At each grid point first-order derivatives are approximated by central differences using the values of the potential from the previous sweep. Thus

$$(G_X)_{i,j} = \frac{1}{2\Delta X} (G_{i+1,j}^o - G_{i-1,j}^o)$$

where i and j are the indices in the X and Y directions, respectively, and the superscript denotes "old" values. A similar expression can be written for G_Y . As a result, velocities are frozen at values of the potential based on the previous sweep. Second-order derivative terms are written taking into account their domain of dependence. At subsonic points central differences are appropriate. The latest values of the potential are used with the current column (j) being relaxed. Thus, if one denotes the difference between the new and old

values by δG_i , then the second-order accurate difference formulas are written as

$$G_{XX} = \frac{1}{\Delta X^2} \left(G_{i+1,j}^0 - 2G_{i,j}^0 + G_{i-1,j}^0 - \frac{2}{\omega} \delta G_{i,j} \right)$$

$$G_{YY} = \frac{1}{\Delta Y^2} \left(G_{i,j+1}^0 - 2G_{i,j}^0 + G_{i,j-1}^0 + \delta G_{i,j+1} - 2\delta G_{i,j} + \delta G_{i,j-1} \right)$$

$$G_{XY} = \frac{1}{4\Delta X\Delta Y} \left(G_{i+1,j+1}^0 - G_{i+1,j-1}^0 - G_{i-1,j+1}^0 + G_{i-1,j-1}^0 \right)$$

where ω is the relaxation factor.

At supersonic points the proper domain of dependence extends upstream. Following Jameson, Ref. 14, the second derivative terms are broken up into their streamwise and normal components as

$$\frac{a^2 - q^2}{q^2} G_{SS} + \frac{a^2}{q^2} G_{NN} = A_1 G_{XX} + A_2 G_{XY} + A_3 G_{YY} \quad (33)$$

and

$$G_{SS} = B_1 G_{XX} + B_2 G_{XY} + B_3 G_{YY}$$

$$G_{NN} = C_1 G_{XX} + C_2 G_{XY} + C_3 G_{YY}$$

where

$$B_1 = \frac{u^2 f X'^2}{r^2}$$

$$B_2 = 2uvf \frac{X'Y'}{r}$$

$$B_3 = v^2 f Y'^2$$

$$C_1 = v^2 f \frac{X'^2}{r^2}$$

$$C_2 = -2uvf \frac{X'Y'}{r}$$

$$C_3 = u^2 f Y'^2$$

The derivatives making up the normal component, G_{NN} , are approximated by the central difference formulas given above with the relaxation factor taken as one. Upwind differencing is used in both the X and Y directions to evaluate the several parts of G_{SS} , the streamwise component. Thus, for example, if $u > 0$ and $v > 0$ the contributions will be

$$G_{XX} = \frac{1}{\Delta X^2} \left(G_{i,j}^0 - 2G_{i,j-1}^0 + G_{i,j-2}^0 + 2\delta G_i \right)$$

$$G_{YY} = \frac{1}{\Delta Y^2} (G_{i,j}^o - 2G_{i,j-1}^o + G_{i,j-2}^o + 2\delta G_j - 2\delta G_{j-1})$$

$$G_{XY} = \frac{1}{2\Delta X\Delta Y} (G_{i,j}^o - G_{i-1,j}^o + G_{i,j-1}^o + G_{i-1,j-1}^o + 2\delta G_j - \delta G_{j-1})$$

Similar expressions can be written for cases where u and v take on different signs. It should be noted that Jameson's rules for balancing "old" and "new" values to provide the right artificial viscosity have been followed.

In order to satisfy the boundary condition at each of the airfoil surfaces a dummy row of points is created beyond each surface. The requirement that there be no flow through the surface at each of the surface grid points ($j = j_s$) can then be met by requiring that the change in potential at the dummy point equal the change at the first point off the surface, that is, $\delta G_{j_{s+1}} = \delta G_{j_{s-1}}$. By this device Φ_r at each surface will remain zero. At the mid-ring boundary, which has been set up to divide the various sweep regions, the values of the potential from the previous pass are kept; essentially this is a Dirichlet-type boundary condition.

By applying these finite-difference relations simultaneously at all grid points on a column extending from either airfoil surface to the mid-ring, a system of linear algebraic equations for the corrections, δG_j is obtained. This system can be represented by

$$[P_{ij}][\delta G_j] = [R_i]$$

It can be easily checked that the matrix $[P_{ij}]$ is tridiagonal and, therefore, can be inverted easily. Sequentially, column by column, all points in the fields are updated, except for the point representing infinity which is kept at its initial value.

At the end of each sweep new values of the circulation can be computed by applying Eq. (30) at each trailing edge and solving the two resulting equations for Γ_1 and Γ_2 . But this expression, which can be rewritten concisely as $\Phi_\theta = 0$, was found to be the source of errors in some cases. Because of the complicated geometries being dealt with in this problem, large circumferential gradients of the potential could appear at one of the trailing edges. For example, there could be a shock or an expansion fan, or both, very near the trailing edge of a slat. For these cases we find the stability to be enhanced by underrelaxation of the evaluation of the circulation constants.

The differencing procedure described above is of a nonconservative form. Although this method produces inaccurate shock "jump" conditions (Refs. 15, 16) generally better agreement with experimental data is obtained. This is likely fortuitous. A completely satisfactory solution would be obtained only with a fully conservative treatment of the inviscid equations together with a proper modeling of the viscous effects and of the shock wave-boundary layer interaction process in particular.

To increase diagonal dominance in the tridiagonal matrix, additional artificial viscosity can be added in the form of a term ϵG_{st} , where t is the time-like coordinate (Ref. 14). With the basic time-like step being the iteration cycle this additional term can be represented by

$$\epsilon G_{st} = \frac{\Delta t}{\Delta \theta} \left(\frac{1}{r} \frac{u}{q} G_{\theta t} + \frac{v}{q} G_{rt} \right)$$

For $v > 0$ this can be put in the form

$$\epsilon G_{st} = \epsilon \left\{ \left[u + rv \frac{\Delta X}{\Delta Y} \frac{Y'}{X'} \right] \delta G_j - \left[rv \frac{\Delta X}{\Delta Y} \frac{Y'}{X'} \right] \delta G_{j-1} - [u (G_{i-1,j} - G_{i-1,j}^0)] \right\}$$

This term is added to the finite-difference analog of Eq. (21). As discussed in Ref. 14, ϵ should be only large enough to ensure convergence. In practice, ϵ has been taken to be zero in most cases.

Finally, in order to improve the computational efficiency, the calculations are performed on a sequence of two grids. The initial (coarse) grid is computed starting with an initial representation of the reduced potential $G(X, Y)$ given by Eq. (31). The starting conditions for the second (fine) grid is obtained by a linear interpolation of the converged coarse grid solution.

5. RESULTS

The method has been applied to a variety of two-element airfoil configurations. Figures 6, 7, 8 show the computed flow field about a NACA 23012 airfoil with a 2-H flap at $M = 0.5$ and an angle of attack of 5° . The calculation was performed using a series of two grids with the final one being 60 (in the circumferential direction) by 30 (in the radial direction). The computed pressure distributions on the main element and flap are shown in Fig. 6, and the computed streamline patterns in the physical and annular domain are shown in Figs. 7 and 8. Imbedded regions of supersonic flow can be seen on the latter graphs. In Fig. 6, the large, "tic" mark on the C_p axis denotes sonic pressure and the sharp nose shock computed is evident.

In this calculation the changes in the reduced potential were converged to 3×10^{-5} on the final grid in approximately five minutes on an IBM 370/168 computer. Some preliminary studies have indicated that the application of the eigenvalue extrapolation method, as discussed in Ref. 8, could substantially improve convergence.

The solution for the flow over a Clark Y airfoil with a 30% Maxwell slat with a gap height of 10% at $M_\infty = 0.6$ is shown in Fig. 9. The supersonic regions in this case are considerably larger. On the slat the entire upper surface flow is supersonic. This results in a large lift being carried by the slat with a significant amount of "rear" loading. The streamline and sonic line patterns in the physical and annular domains are shown in Figs. 10 and 11.

A still larger supersonic region occurs in the next example which shows a slatted configuration that is obtained from a modified NACA 64A008 section profile at $M_\infty = 0.7$ and $\alpha = 6^\circ$. The computed pressure distribution and streamline contours are shown in Figs. 12 and 13. Even though the present grid is not as dense as those used in the single-element computations, the shock is clearly defined. It should be kept in mind that the flow on the lower surface of the slat could separate so that some of the lift shown being carried by the slat could be lost. A calculation for the $M_\infty = 0.8$, $\alpha = 4^\circ$ flow over a slatted configuration based on a modified NACA 64A009 airfoil is presented in Fig. 14. A plot of the Mach number contours illustrating the large regions of supersonic flow is given in Fig. 15.



Fig. 6 Computed Surface Pressure Distribution NACA 23012 Airfoil/2H Flap, $M_\infty = 0.5$, $\alpha = 4^\circ$

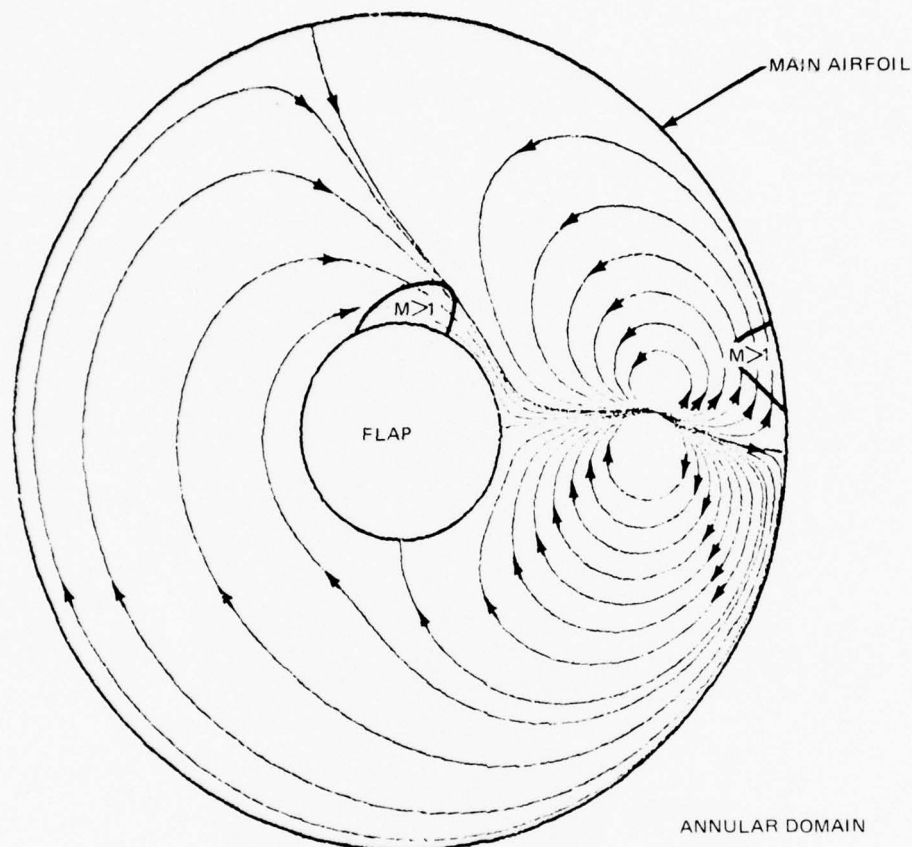


Fig. 7 Computed Streamlines – Annular Domain NACA 23012 Airfoil/2H Flap, $M_\infty = 0.5$, $\alpha = 4^\circ$

The choice of sweep directions causes no difficulties for cases where a supersonic region should span the entire gap between the two elements. This situation occurs for the slatted NACA 0012 airfoil at $M_\infty = 0.6$ and $\alpha = 4^\circ$ as seen in Fig. 16. Here Mach number contours are plotted with the sonic line being marked more heavily. The corresponding pressures are shown in Fig. 17. The supersonic region spanning the gap is swept in the streamline direction along both surfaces so that the proper domain of dependence is maintained.

A final example provides some measure of the performance of the method. Figure 18 depicts the computed pressures and experimental data for the geometry shown. The geome-

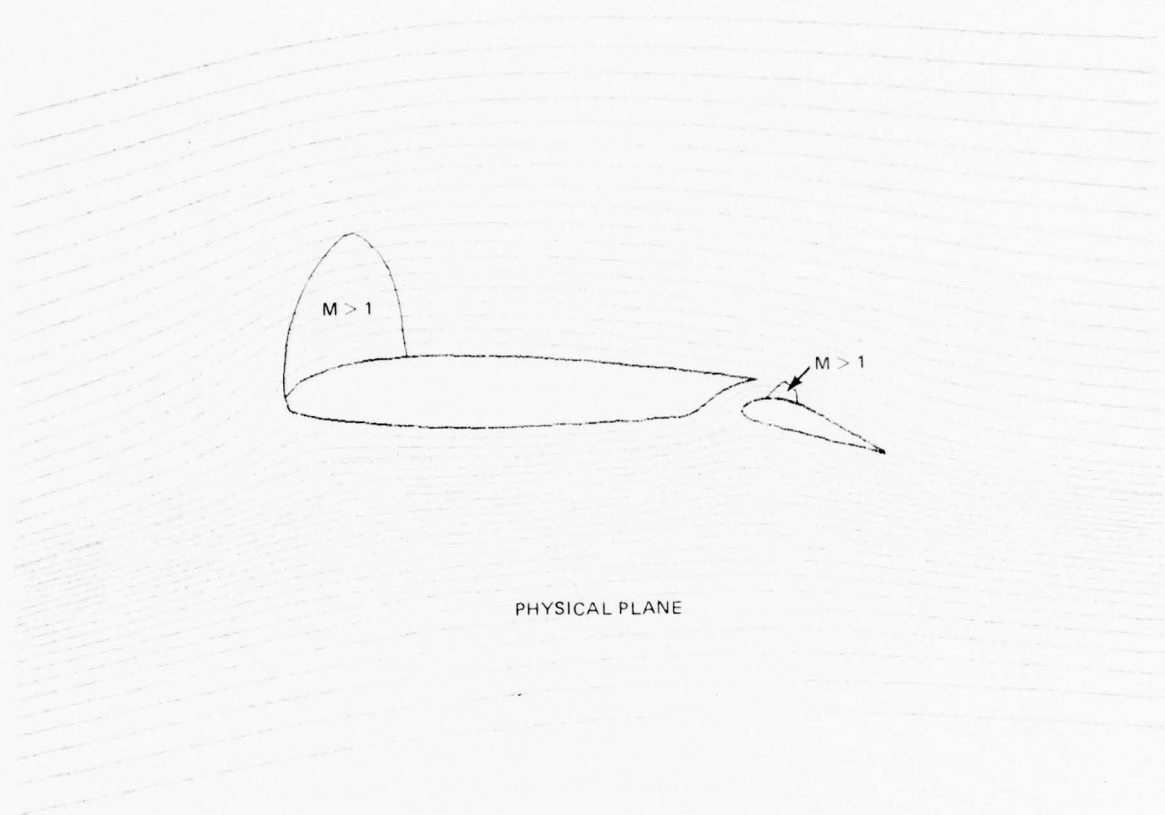


Fig. 8 Computed Streamlines — Physical Plane NACA 23012 Airfoil/2H Flap, $M_\infty = 0.5$, $\alpha = 4^\circ$

try used in the computation is the 64A406 airfoil with 7.8 A slat configuration tested, corrected through the addition of a nominal displacement thickness. The overall agreement is not very good and this implies that the boundary layer correction applied to the ordinates was insufficient. The excellent agreement and the lower surface suggests that discrepancies on the upper surface of the main airfoil and on the slat are due to the trailing-edge separation on the main foil and separation on the lower surface of the slat. The disagreement between the numerical solution and the data on the upper surface of the main element consists mainly of an upward shift. Despite the shift all the features of the flow are predicted by the computation including the double peak occurring near the nose of the main foil. The agreement would undoubtedly be improved by properly accounting for viscous effects. As shown in Fig. 19, the sonic region not only spans the entire gap but also touches the trailing edge of the slat. With the particular differencing scheme used in the application of the Kutta conditions the method had no difficulty computing the rapid expansion around the trailing edge of the slat.

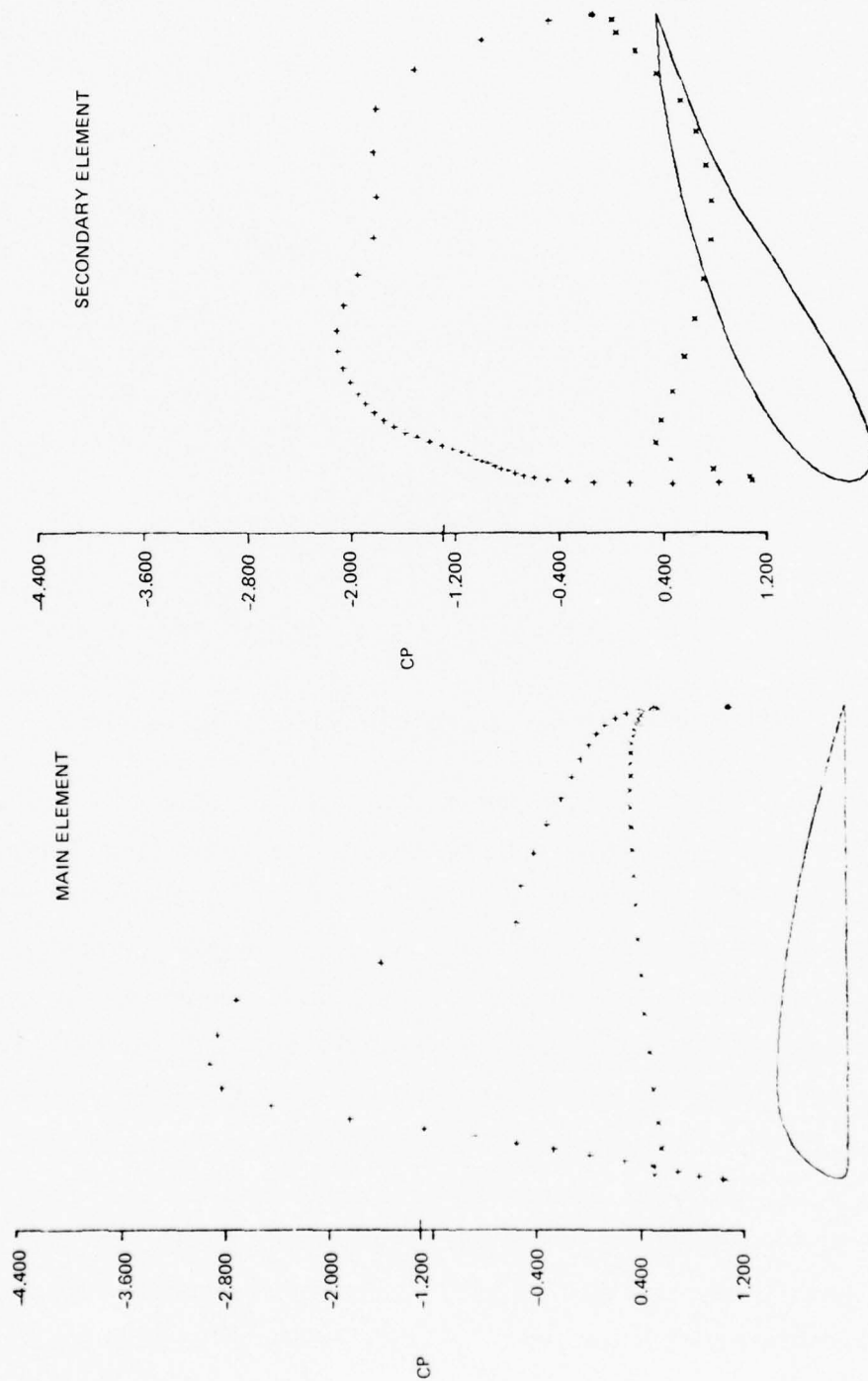


Fig. 9 Computed Surface Pressure Distribution Clark Y Airfoil/30% Maxwell Slat, $M_{\infty} = 0.6$, $\alpha = 6^\circ$

CD.

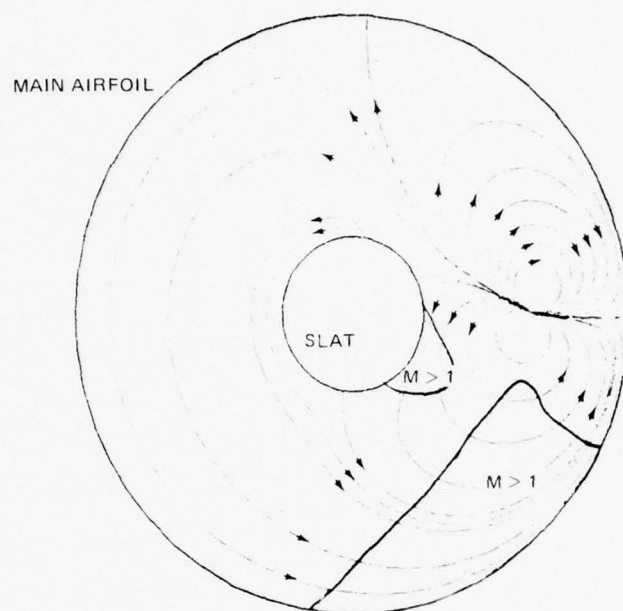


Fig. 10 Computed Streamlines — Annular Domain Clark Y Airfoil/30% Maxwell Slat, $M_\infty = 0.6$, $\alpha = 6^\circ$

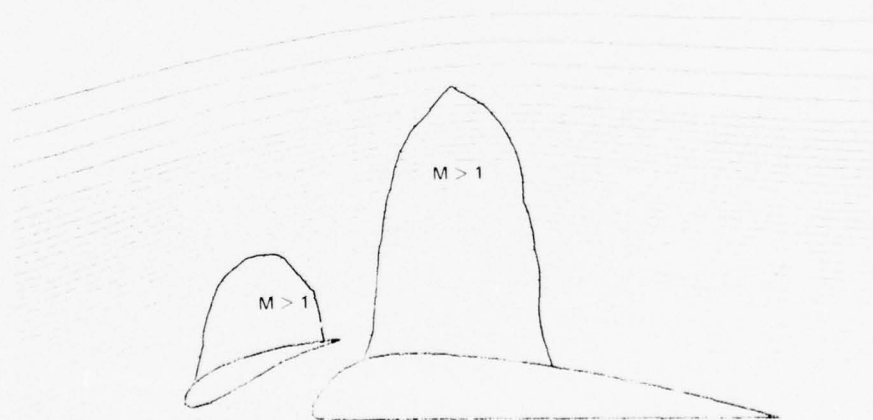


Fig. 11 Computed Streamlines — Physical Plane Clark Y Airfoil/30% Maxwell Slat, $M_\infty = 0.6$, $\alpha = 6^\circ$

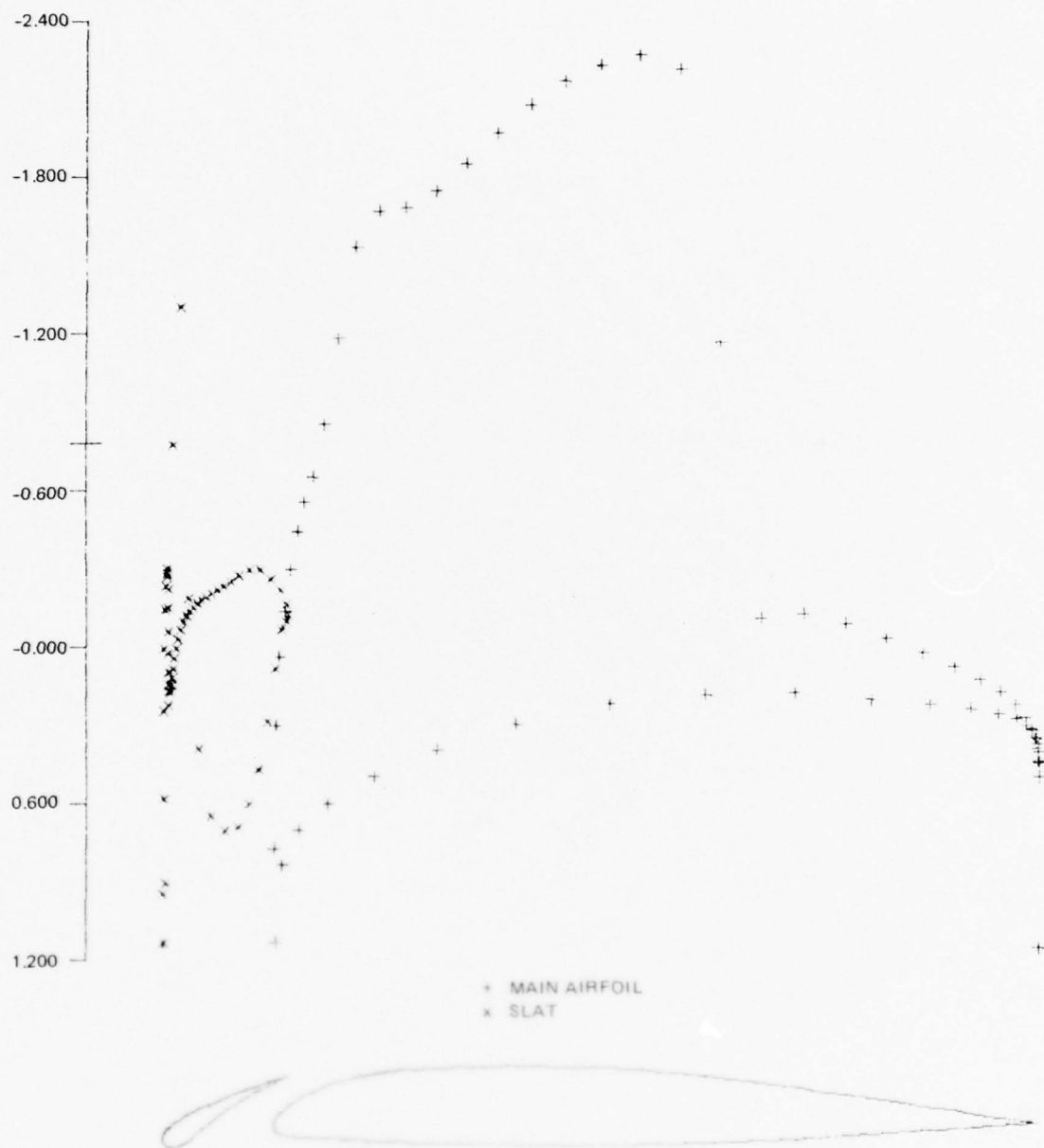


Fig. 12 Computed Surface Pressure Distribution Modified NACA 64A008 Airfoil/Slat, $M = 0.7$, $\alpha = 6^\circ$

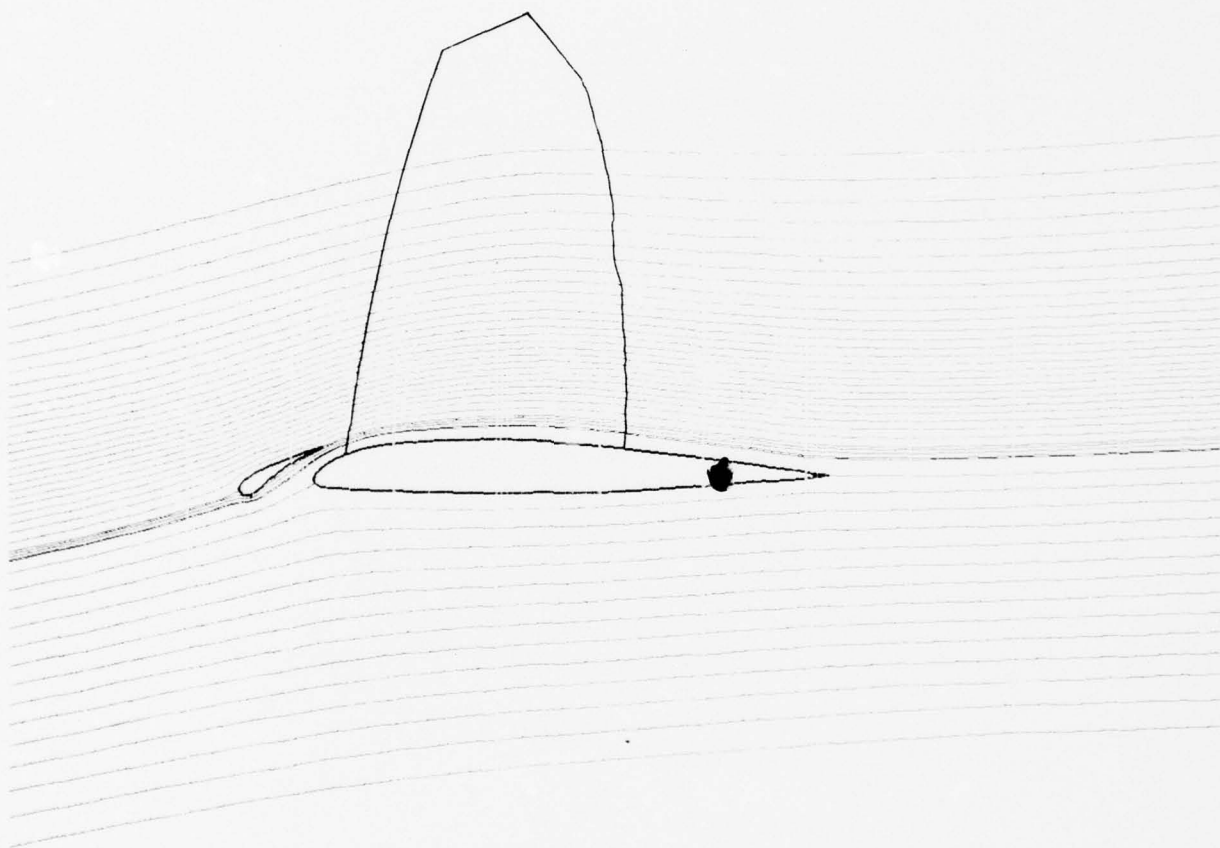


Fig. 13 Computed Streamlines – Physical Domain Modified NACA 64A008 Airfoil/Slat, $M = 0.7$, $\alpha = 6^\circ$

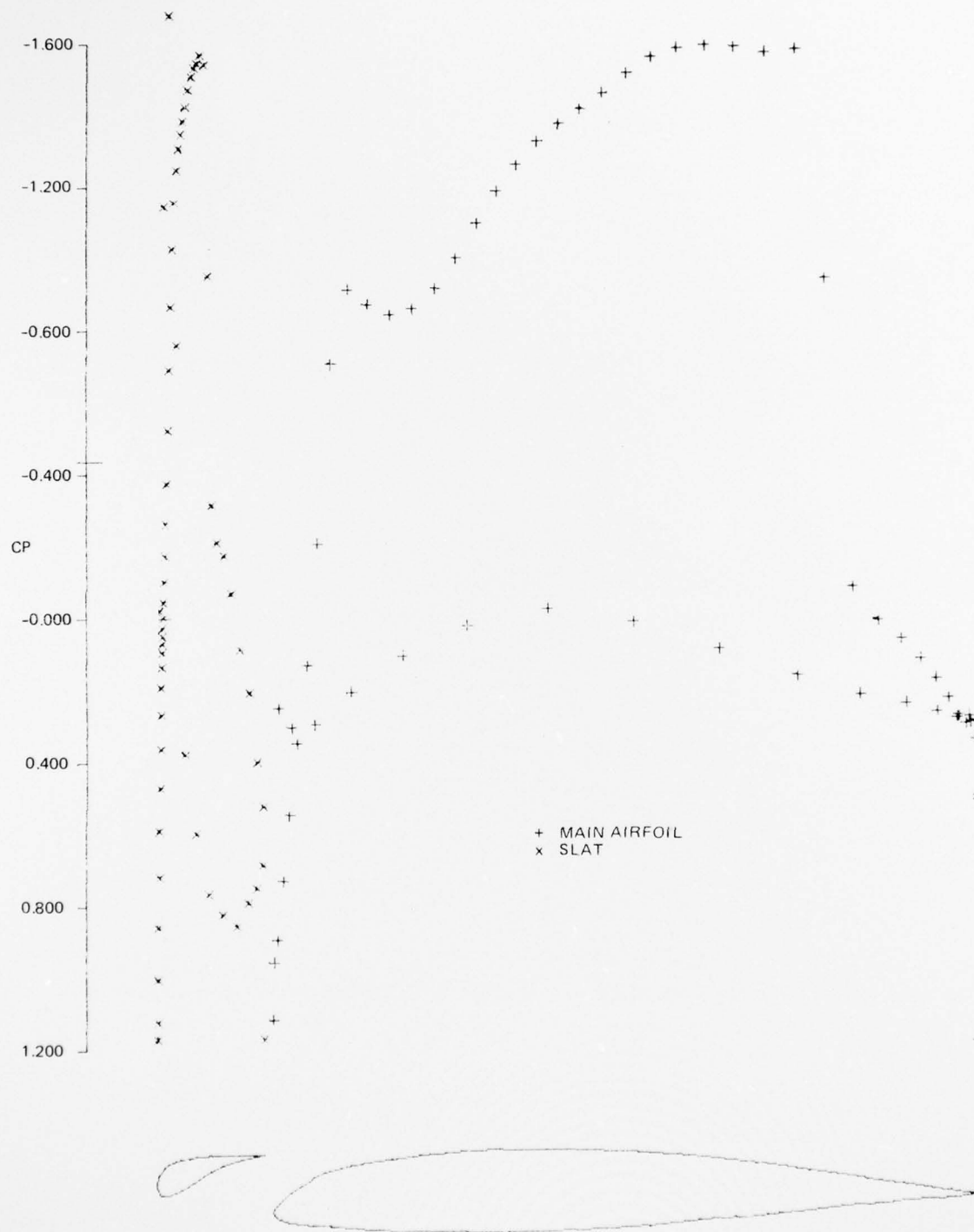


Fig. 14 Computed Surface Pressure Distribution Modified NACA 0009 Airfoil/Slat, $M_\infty = 0.8$, $\alpha = 4^\circ$

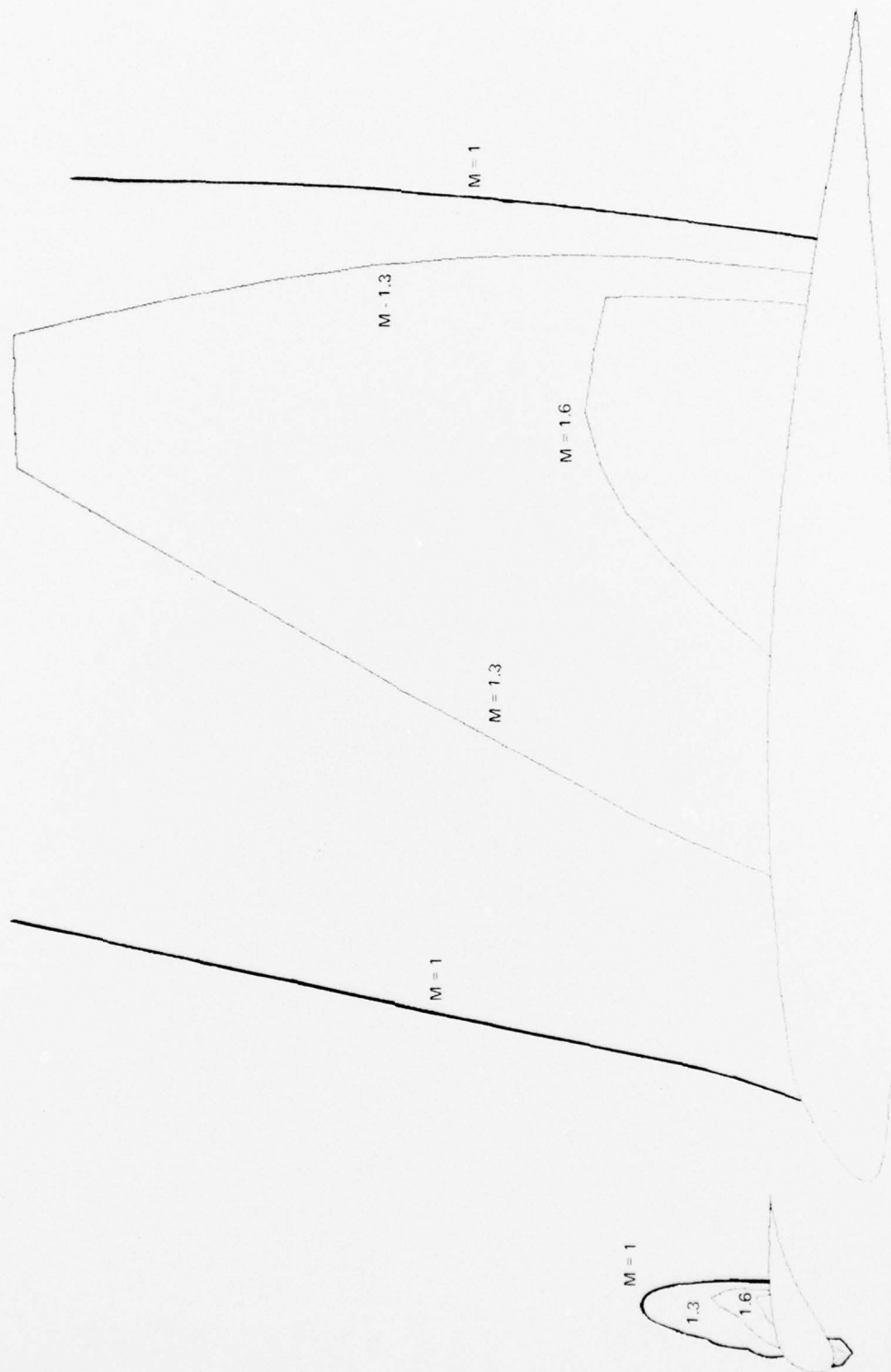


Fig. 15 Mach Number Contours Modified NACA 64A009 Airfoil/Slat, $M_\infty = 0.8$, $\alpha = 4^\circ$



Fig. 16 Mach Number Contours NACA 0012 Airfoil and Slat, $M_\infty = 0.6$, $\alpha = 4^\circ$

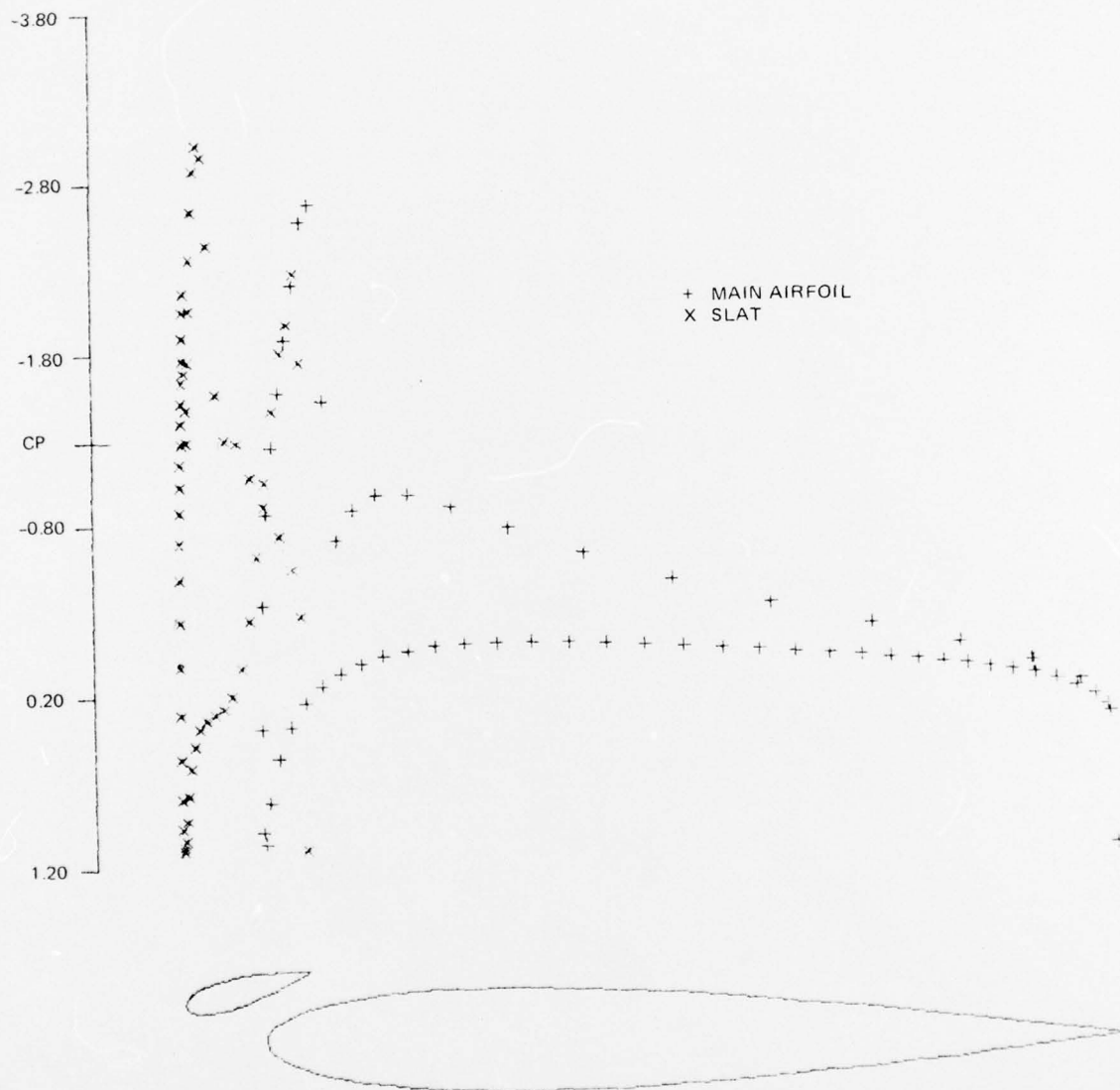


Fig. 17 Computed Surface Pressure Distribution NACA 0012 Airfoil and Slat, $M_\infty = 0.6$, $\alpha = 4^\circ$

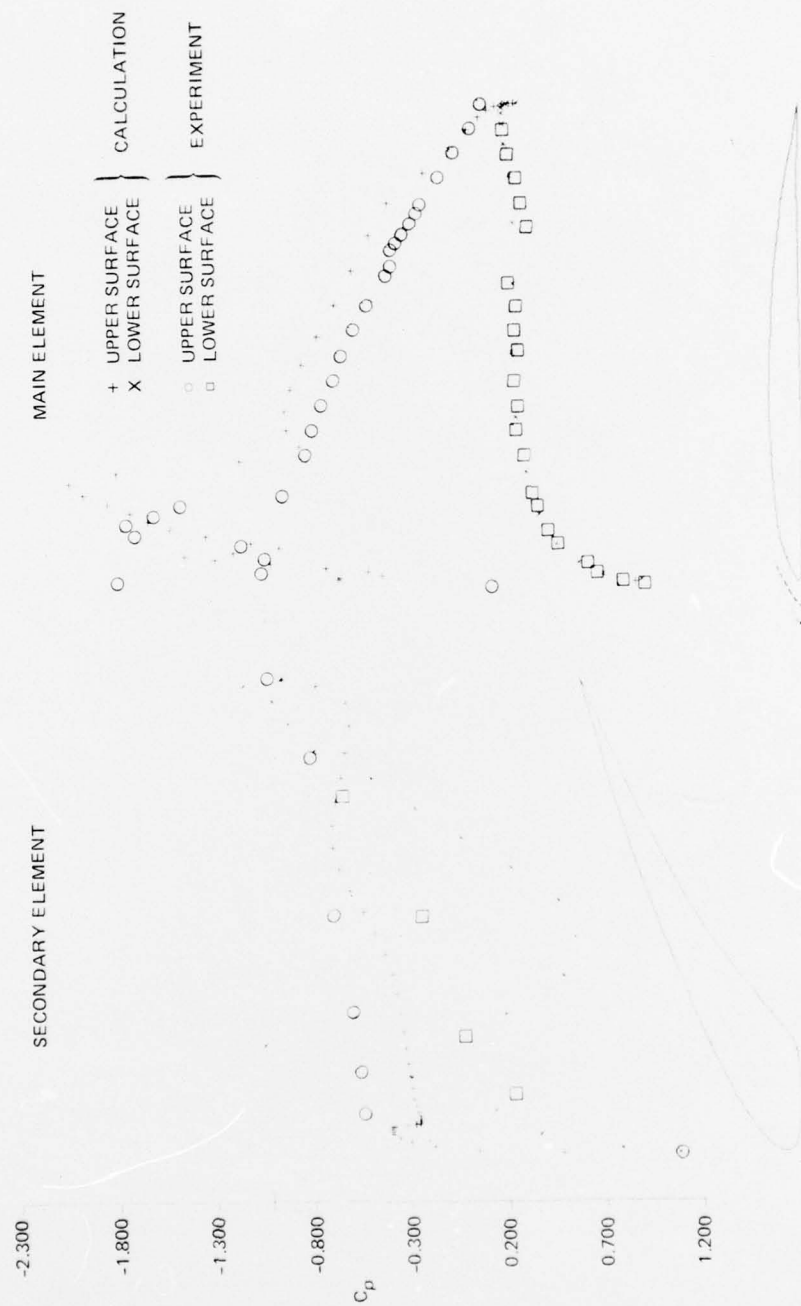


Fig. 18 Computed Surface Pressure Distribution NACA 64A406/7.8A Slat, $M = 0.649$, $\alpha = 4^\circ$



Fig. 19 Mach Number Contours NACA 64A406 Airfoil/7.8A Slat, $M_{\infty} = 0.649$, $\alpha = 4^{\circ}$

6. CONCLUSIONS

A numerical method has been developed to calculate the inviscid transonic flow over arbitrary two-element airfoil systems. Conformal mapping procedures were utilized to develop a convenient computational domain where boundary conditions on the airfoil surfaces and at infinity could be accurately prescribed and with appropriate spatial grid definition to account for steep flow gradients. The exact irrotational flow equations were derived in terms of a smoothly varying single-valued reduced potential in the computational domain. A stable, accurate and efficient finite-difference procedure was developed using mixed-flow relaxation techniques. The numerical method was applied to a variety of airfoils with leading-edge slats and trailing-edge flaps over a range of free-stream Mach numbers and angles of attack.

Our computed results indicate the ability of the method to compute inviscid transonic flows over two-element airfoil configurations. One aspect of this effort which requires further study is the improvement of the computational efficiency. We have preliminary computations with the eigenvalue extrapolation procedure of Ref. 8, which indicate a possible 40% reduction of iteration cycles. This technique will be implemented in the near future.

Another area of further study is the verification of the accuracy of our method by comparison with experimental data. However, it is evident that transonic two-element airfoil flows are strongly influenced by viscous effects. Thus, we are in the process of including boundary layer effects in our computational technique. Special emphasis will be given to including strong viscous interaction effects at trailing edges, shock waves, and in regions of separated flow.

We also intend to reformulate the problem in the design (inverse) mode, whereby the pressure distribution will be prescribed over all or parts of the airfoil surfaces and the ordinates will evolve as part of the solution procedure. Techniques developed for single-element design, such as Ref. 17, will be utilized.

7. REFERENCES

1. Caughey, D., "An Inviscid Analysis of Transonic, Slatted Airfoils," AIAA Paper no. 74-541, 1974.
2. Murman, E. M. and Cole, J. D., "Calculation of Plane Steady Transonic Flows," AIAA J., Vol. 9, 1971.
3. Jameson, A., "Transonic Flow Calculations for Airfoils and Bodies of Revolution," Grumman Aerospace Corporation, Aerodynamics Report 390-71-1, 1971
4. Garabedian, P. R. and Korn, D. G., "Analysis of Transonic Airfoils," Comm. Pure Appl. Math., Vol. 24, 1971.
5. South, J. C. Jr. and Jameson, A., "Relaxation Solutions for Inviscid Axisymmetric Transonic Flows over Blunt or Pointed Bodies," Proceedings of the AIAA Computational Fluid Dynamics Conference, pp. 8-17, 1973.
6. Grossman, B. and Melnik, R. E., "The Numerical Computation of the Transonic Flow over Afterbodies Including the Effect of Jet-Plume and Viscous Interactions," AIAA Paper 75-62, 1975.
7. Arlinger, B. G., "Calculation of Transonic Flow around Axisymmetric Inlets," AIAA Paper 75-80, 1975.
8. Caughey, D. A. and Jameson, A., "Accelerated Iterative Calculation of Transonic Nacelle Flow Fields," AIAA Paper 76-100, 1976.
9. Grossman, B. and Melnik R. E., "The Numerical Computation of the Transonic Flow Over Two-Element Airfoil Systems," Proceedings of the Fifth International Conf. on Numerical Methods in Fluid Dynamics, Springer-Verlag, pp. 220-337, June 1976.
10. Arlinger, B. G., "Analysis of Two Element High Lift Systems in Transonic Flow," ICAS Paper, 1976.
11. Ives, D. C., "A Modern Look at Conformal Mapping, Including Doubly Connected Regions," AIAA Paper 75-842, 1975.
12. Ludford, G. S. S., "The Behavior at Infinity of the Potential Function of a Two Dimensional Subsonic Compressible Flow," J. Math. Phys. Vol. 30, 1951.
13. Lagally, M., "Die Reibungslose Stromung in Aussengebiete Zwier Kreise," ZAMM, Vol. 9, No. 4, pp 209-305, (Translated in NACA 626) 1929.
14. Jameson, A., "Iterative Solution of Transonic Flow Over Airfoils and Wings, Including Flows at Mach 1," Comm. Pure and Appl. Math., Vol. 27, 1974.
15. Murman, E. M., "Analysis of Embedded Shock Waves Calculated by Relaxation Methods," AIAA J., Vol. 12, No. 5, 1974.
16. Newman, P. A. and South, J. C. Jr., "Conservative Versus Nonconservative Differencing: Transonic Streamline Shape Effects," NASA TMX 72827, 1976.
17. Volpe, G., "Recent Advances in Airfoil Analysis and Design," Grumman Aerodynamics Memorandum 75-27, 1975.

APPENDIX
Evaluation of the Z_3 - Z_4 Mapping Coefficients

We discuss in detail the mapping from the Z_3 to the Z_4 plane as given in Eq. (3). In order to determine the coefficients of this mapping we consider the following preliminary mapping

$$g = f^{1/\kappa} \quad (\text{A. 1a})$$

$$g = \frac{(\xi - c)\left(\xi - \frac{1}{\bar{c}}\right)}{(\xi - d)\left(\xi - \frac{1}{\bar{d}}\right)} \quad (\text{A. 1b})$$

$$f = \frac{(z - a)\left(z - \frac{1}{\bar{a}}\right)}{(z - b)\left(z - \frac{1}{\bar{b}}\right)} \quad (\text{A. 1c})$$

where c and d are the unknown coefficients.

On the unit circle $z\bar{z} = 1$, f may be written as

$$f = \left| \frac{z - a}{z - b} \right|^2 \frac{\bar{b}}{\bar{a}}$$

so that the unit circle in the z plane maps to a slit in the f plane at an angle $\arg(\bar{b}/\bar{a})$ with end points at f_1 and f_2 where $\left| \frac{z - a}{z - b} \right|$ reaches its extreme values. Then through the mapping (A. 1a) we get another slit stretching from $(f_1)^{1/\kappa}$ to $(f_2)^{1/\kappa}$. Now the mapping (A. 1b) maps a unit circle in the ξ plane ($\xi\bar{\xi} = 1$) to a slit between g_1 and g_2 . Thus, if we choose c and d so that

$$\begin{aligned} g_1 &= f_1^{1/\kappa} \\ g_2 &= f_2^{1/\kappa} \end{aligned} \quad (\text{A. 2})$$

then the unit circle in the z plane will be mapped to a unit circle in the ξ plane. To make the slits collinear requires

$$\arg\left(\frac{c}{d}\right) = \frac{1}{\kappa} \arg\left(\frac{a}{b}\right) \quad (\text{A. 3})$$

Then c and d must be chosen so that g_1 and g_2 have the magnitude appropriate to Eq. (A. 2).

To determine g_1 and g_2 take $\tilde{c} = 1/\bar{c}$, $\tilde{d} = 1/\bar{d}$ and evaluate

$$\frac{1}{g} \frac{dg}{d\xi} = \frac{1}{\xi - c} + \frac{1}{\xi - \tilde{c}} - \frac{1}{\xi - d} - \frac{1}{\xi - \tilde{d}} = \frac{c-d}{(\xi-c)(\xi-d)} + \frac{\tilde{c}-\tilde{d}}{(\xi-\tilde{c})(\xi-\tilde{d})} = 0 \quad (\text{A. 4})$$

The ends of the slit are the branch points g_1 and g_2 where $\frac{dg}{d\zeta}$ vanishes. Thus, at a branch point ζ satisfies

$$\begin{aligned} 0 &= (\zeta - \tilde{c})(\zeta - \tilde{d})(c - d) + (\zeta - c)(\zeta - d)(\tilde{c} - \tilde{d}) \\ &= A\zeta^2 - B\zeta + C \end{aligned} \quad (\text{A.5a})$$

where

$$A = (c + \tilde{c}) - (d + \tilde{d}) \quad (\text{A.5b})$$

$$B = 2(c\tilde{c} - d\tilde{d}) \quad (\text{A.5c})$$

$$C = c\tilde{c}(d + \tilde{d}) - d\tilde{d}(c + \tilde{c}) \quad (\text{A.5d})$$

Then if ζ_1 and ζ_2 are the roots of the branch points, g_1 and g_2 are given by

$$g_j = \frac{(\zeta_j - c)(\zeta_j - \tilde{c})}{(\zeta_j - d)(\zeta_j - \tilde{d})}, \quad j = 1, 2 \quad (\text{A.6})$$

The expressions for the branch points f_1, f_2 may be evaluated in an analagous manner. Now from condition (A.1a)

$$g_1 g_2 = (f_1 f_2)^{1/\kappa} \quad (\text{A.7})$$

Utilizing Eqs. (A.5) we obtain $\zeta_1 \zeta_2 = \frac{C}{A}$ and $\zeta_1 + \zeta_2 = \frac{B}{A}$ and with Eq. (A.6) we can develop (after some tedious algebra) that

$$g_1 g_2 = \left(\frac{c - \tilde{c}}{d - \tilde{d}} \right)^2 = \left[\frac{(|c|^2 - 1)}{(|d|^2 - 1)} \frac{\tilde{d}}{\tilde{c}} \right]^2 \quad (\text{A.8})$$

and an analagous expression for $f_1 f_2$. Thus, Eq. (A.7) requires that

$$\frac{c - \tilde{c}}{d - \tilde{d}} = \left(\frac{a - \tilde{a}}{b - \tilde{b}} \right)^{1/\kappa} \quad (\text{A.9})$$

Now the branch point condition Eq. (A.4) may be rewritten as

$$0 = \frac{(2\zeta - c - \tilde{c})}{(\zeta - c)(\zeta - \tilde{c})} - \frac{(2\zeta - d - \tilde{d})}{(\zeta - d)(\zeta - \tilde{d})} \quad (\text{A.10})$$

and the branch point g_1 given in Eq. (A.6) becomes

$$g_1 = \frac{c + \tilde{c} - 2\zeta_1}{d + \tilde{d} - 2\zeta_1} \quad (\text{A.11})$$

However ζ_1 lies on the unit circle, and we are free to rotate the ζ plane so that the $\arg(\zeta_1)$ takes any desired value. Thus, if we assign a value for ζ_1 , the condition

$$g_1 = (f_1)^{1/\kappa} \quad (\text{A.12})$$

gives one relationship for $c, d, \tilde{c}, \tilde{d}$ and Eq. (A.9) gives a second; and since \tilde{c} and \tilde{d} are determined from c and d we have two equations for c and d .

These equations may be developed in a convenient form by noting that

$$f_1 = \frac{(z_1 - a)(z_1 - \bar{a})}{(z_1 - b)(z_1 - \bar{b})} = \left| \frac{z_1 - a}{z_1 - b} \right|^2 \frac{\bar{b}}{\bar{a}} \quad (\text{A. 13})$$

while according to (A. 9) we define a quantity E as

$$E \equiv \frac{c - \bar{c}}{d - \bar{d}} = \left(\frac{a - \bar{a}}{b - \bar{b}} \right)^{1/\kappa} = \left\{ \left(\frac{|a|^2 - 1}{|b|^2 - 1} \right) \frac{\bar{b}}{\bar{a}} \right\}^{1/\kappa} \quad (\text{A. 14})$$

Thus

$$\begin{aligned} f_1^{1/\kappa} &= \left\{ \left| \frac{z_1 - a}{z_1 - b} \right|^2 \left(\frac{|b|^2 - 1}{|a|^2 - 1} \right) \right\}^{1/\kappa} E \\ &= \beta E \end{aligned} \quad (\text{A. 15})$$

The two equations for c and d are obtained from Eqs. (A. 9) and (A. 10) utilizing Eqs. (A. 14) and (A. 15) as

$$c - \frac{1}{\bar{c}} = E \left(d - \frac{1}{\bar{d}} \right) \quad (\text{A. 16})$$

$$c + \frac{1}{\bar{c}} = D + \beta E \left(d + \frac{1}{\bar{d}} \right) \quad (\text{A. 17})$$

where $D \equiv 2\zeta_1(1 - \beta E)$ and ζ_1 has an assigned value on the unit circle. Combining the above two equations we obtain

$$2c = D + \beta E \left(d + \frac{1}{\bar{d}} \right) + E \left(d - \frac{1}{\bar{d}} \right) \quad (\text{A. 18})$$

$$\frac{2}{\bar{c}} = D + \beta E \left(d + \frac{1}{\bar{d}} \right) - E \left(d - \frac{1}{\bar{d}} \right) \quad (\text{A. 19})$$

We can also note that by definition

$$\arg \left(c + \frac{1}{\bar{c}} \right) = \arg \left(c - \frac{1}{\bar{c}} \right) = \arg(c)$$

$$\arg \left(d + \frac{1}{\bar{d}} \right) = \arg \left(d - \frac{1}{\bar{d}} \right) = \arg(d)$$

whereby Eqs. (A. 16) and (A. 17) yield

$$\arg(c) = \arg(Ed) = \arg(D) \quad (\text{A. 20})$$

Taking the complex conjugate of Eq. (A. 18) and multiplying by Eq. (A. 19) and simplifying the expression using Eq. (A. 20) gives the following

$$\left(|D| + \beta |E| \left| d + \frac{1}{\bar{d}} \right| \right)^2 - |E|^2 \left| d - \frac{1}{\bar{d}} \right|^2 = 4 \quad (\text{A. 21})$$

Letting $r \equiv |E| \left| d + \frac{1}{\bar{d}} \right|$ we obtain

$$(|D| + \beta r)^2 - r^2 + 4|E|^2 = 1 \quad (\text{A. 22})$$

which may easily be solved since D and E are known. Then

$$|d| + \frac{1}{|d|} = \frac{r}{|E|}$$

whereby

$$|d| = \frac{r}{2|E|} + \sqrt{\frac{r^2}{4|E|^2} - 1} \quad (\text{A.23})$$

where the root larger than 1 has been chosen. Also from Eq. (A.20)

$$\arg(d) = \arg(D/E) \quad (\text{A.24})$$

and thus Eqs. (A.23) and (A.24) determine d and c may then be found from Eq. (A.16).

The mapping coefficients found completely determine the mapping given by Eqs. (A.1). This mapping differs from the one developed by Ives (Ref. 11) and given in Eq. (3) by a scale transformation. If we define

$$S \equiv \kappa \left[\frac{c + \frac{1}{c} - d - \frac{1}{d}}{a + \frac{1}{a} - b - \frac{1}{b}} \right] \quad (\text{A.25})$$

Then Eqs. (A.1) are identical to Eq. (3) with

$$Z_4 = \xi/S$$

$$Z_{4T} = c/S$$

$$Z_{4N} = d/S$$

$$r_s^2 = S\bar{S}$$

and

$$Z_3 = z$$

$$Z_{3T} = a$$

$$Z_{3N} = b$$

$$\kappa_2 = \kappa$$

Thus we have reduced the determination of the mapping coefficients of Eq. (3) to the solution of two real quadratic equations. In Ref. 11, these mapping coefficients are found using a complicated three-dimensional Newton-Rapheson iteration process.

DISTRIBUTION LIST

Chief of Naval Research
Department of the Navy
Arlington, VA 22217
ATTN: Vehicles and Propulsion
Program, Code 211
Code 430B

Chief of Naval Development
Department of the Navy
Washington, DC 20360
ATTN: NAVMAT 0331
NAVMAT 0334

Naval Air Systems Command
Department of the Navy
Washington, DC 20351
ATTN: NAVAIR 3200
NAVAIR 5301
NAVAIR 53013

David Taylor Naval Ship Research
& Development Center
Bethesda, MD 20084
ATTN: Code 16
Code 522.3
Code 522.1

Naval Research Laboratory
Washington, DC 20375
ATTN: Technical Information
Office, Code 2627
Library, Code 2629

Superintendent
U.S. Naval Academy
Annapolis, MD 21402

Superintendent
U.S. Naval Postgraduate School
Monterey, CA 93940

U. S. Naval Air Development Center
Warminster, PA 18974
Air Vehicle Technology Dept.
ATTN: Code 301

ONR Branch Office
1030 East Green Street
Pasadena, CA 91106
ATTN: Mr. B. F. Cagle

ONR Branch Office
495 Summer Street
Boston, MA 02210
ATTN: Dr. A. D. Wood

ONR Branch Office
536 South Clark Street
Chicago, IL 60605
ATTN: Mr. M. A. Chaszeyka

Commandant of the Marine Corps
Washington, DC 20380
ATTN: Dr. A. L. Slafkosky
Scientific Advisor
(Code RD-1)

Defense Documentation Center
Cameron Station, Bldg. 5
Alexandria, VA 22314

Department of the Army
DCS for Research and Development and
Acquisition
Washington, DC 20310
ATTN: DAMA-WSA (Mr. R. L. Ballard)

U.S. Army Material Command
5001 Eisenhower Avenue
Alexandria, VA 22333
ATTN: AMCRD-F

Director, Headquarters
U.S. Army Air Mobility R&D Lab.
Ames Research Center
Moffett Field, CA 94035

Director, Ames Directorate
U. S. Army Air Mobility R&D Lab.
Ames Research Center
Moffett Field, CA 94035

5

1

1

1

1

1

1

1

1

1

1

1

1

1

1

1

1

1

1

12

1

1

1

1

Director, Langley Directorate U. S. Army Air Mobility R&D Lab. Langley Research Center Hampton, VA 23665	1	Lockheed Missiles & Space Co., Inc. Huntsville Research & Engineering Center P. O. Box 1103 Huntsville, AL 35807 ATTN: Mr. A. Zalay	1
Director, Eustis Directorate U. S. Army Air Mobility R&D Lab. Fort Eustis, VA 23604	1	Rockwell International Science Center Thousand Oaks, CA 91360 ATTN: Dr. N. Malmuth	1
U. S. Air Force Flight Dynamics Laboratory Wright-Patterson AFB, OH 45433 ATTN: PR, Prototype Division	1	Nielsen Engineering & Research, Inc. 510 Clyde Avenue Mountain View, CA 94043	1
FXM, Aeromechanics Branch	1		
Air Force Office of Scientific Research Directorate of Aerospace Sciences Bolling AFB, DC 20332	1	University of Cincinnati Department of Aerospace Engineering and Applied Mechanics Cincinnati, OH 45221 ATTN: Dr. R. T. Davis	1
National Aeronautics and Space Administration 600 Independence Avenue, SW Washington, DC 20546 ATTN: Code RAA	1		
Code RAV	1		
National Aeronautics and Space Administration Ames Research Center Moffett Field, CA 94035 ATTN: Dr. T. Gregory	1		
Dr. G. Chapman	1		
National Aerodynamics and Space Administration Langley Research Center Hampton, VA 23665 Subsonic, Transonic Aerodynamics Div. ATTN: Dr. James F. Campbell	1		
Dr. Stephen Wornom	1		
Flow Research, Inc. 1819 South Central Avenue Kent, WA 98031 ATTN: Dr. E. Murman	1		